SENSING AND SEPARATING BIOMOLECULES AT BIOINTERFACES

A Dissertation

by

HYUNSOOK JUNG

Submitted to the Office of Graduate Studies of
Texas A&M University
in partial fulfillment of the requirements for the degree of

DOCTOR OF PHILOSOPHY

May 2009

Major Subject: Chemistry

SENSING AND SEPARATING BIOMOLECULES AT BIOINTERFACES

A Dissertation

by

HYUNSOOK JUNG

Submitted to the Office of Graduate Studies of
Texas A&M University
in partial fulfillment of the requirements for the degree of

DOCTOR OF PHILOSOPHY

Approved by:

Chair of Committee,	Paul S. Cremer
Committee Members,	Gregory D. Reinhart
	Emile A. Schweikert
	James D. Batteas
Head of Department,	David H. Russell

May 2009

Major Subject: Chemistry

ABSTRACT

Sensing and Separating Biomolecules at Biointerfaces. (May 2009)

Hyunsook Jung, B.S., Hanyang University; M.S., Korea Advanced Institute of Science and Technology

Chair of Advisory Committee: Dr. Paul S. Cremer

Ligand-receptor interactions are ubiquitous on cell membranes. Indeed, many important physiological functions primarily involve such interactions. These include cell signaling, pathogen binding, trafficking of lymphocytes, and the immune response.[1-4] Therefore, studying ligand-receptor interactions at appropriate model membrane is of importance for both proper understanding of biological functions and applications to biosensors and bioseparations.

Supported lipid bilayers are composed of the same lipid molecules found in the plasma cell membranes of living cells and possess the same two-dimensional fluidity as cell membranes, making them capable of mimicking the cell surface. Moreover, supported lipid bilayer-based in vitro assays are appealing because they require only very small sample volumes and they are suitable for multiplexing and high-throughput screening.

Recently, our laboratory has combined supported lipid bilayer-coated microfluidic platforms with total internal reflection fluorescence microscopy to obtain equilibrium dissociation constant data for protein-ligand interactions. Using this method,

it was found that equilibrium dissociation constants of antibody-ligand interactions at lipid membrane interfaces can be strongly affected by ligand lipophilicity and linker length/structure. These results are described in Chapter III.

Monitoring protein-ligand interactions is routinely performed by fluorescently labeling the proteins of interest. Protein labeling can, however, interfere with detection measurements and be highly inconvenient to employ. To solve these problems, a simple and highly sensitive technique for detection of protein-ligand binding at biointerfaces has been developed. The method is based upon modulation of the interfacial pH when the protein binds. This change is detected by pH-sensitive fluorescent dye molecules embedded into the biointerface. The dye fluoresces strongly in the protonated state but becomes inactive upon deprotonation. These results are demonstrated in Chapter IV.

Finally, the study of supported lipid bilayer-based electrophoresis is described in Chapter V. Bilayer electrophoresis is an attractive alternative to gel electrophoresis for the separation of membrane components such as lipids and membrane proteins because it is run in native-like environments and avoids exposing the analytes of interest to harsh chemicals. In this study, lipid rafts of varying size were used as separation matrices to separate two similar lipids with different alkyl chains. Lipid rafts of varying size were formed by a process controlled by varying treatment of the solid substrate. Depending on which method was employed, the results showed that lipid raft size could be modulated over five orders of magnitude. Moreover, it was found that the electrophoretic separation of the two lipid components depended on the size of rafts in the bilayer matrix.

DEDICATION

To my parents, Seunghee Jung and Kyungsoon Kim

To my husband, Hoon Yim

And to my daughters, Dahee Yim and Eunjee Yim

ACKNOWLEDGEMENTS

Particular thanks are due to my advisor, Prof. Paul S. Cremer, and my committee members, Prof. Greogry D. Reinhart, Prof. Emile A. Schweikert, and Prof. James D. Batteas, for their guidance and support throughout the course of this research.

Thanks also go to my friends (Jun Yong Kang, Hejin Lee, Youngbok Lee, and Ming-Chien Li), colleagues (Dr. Tinglu Yang, Dr. Jinjun Shi, Dr. Mauricio D. Lasagna, Dr. Laura B. Sagle, Dr. Xin Chen, Aaron D. Robison, Jixin Chen, Younhee Cho, Dr. Yanjie Zhang, Sean Bard, Chin-Yuan Chang, Sarah Flores, Jaibir Kherb, Wei-Ssu Liao, Chunming Liu, Hudson Pace, Dr Arnaldo Diaz, Dr. Susan Daniel, Dr. Soon-Mi Lim, Vanessa Chapa Fruchey, Dr. Sho Kataoka**,** Dr. Edward Castellana, Dr**.** Fernando Albertorio, Dr. Katherine Cimatu, and Dr. Christopher F. Monson), department faculty (Dr. Dong Hee Son, Dr. Gyula Vigh, and Dr. Simon W. North, and Dr. Wendy Keeney-Kennicut) and staff (Ms. Sandy Manning, Ms. Lea Mueschke, and Ms. Jennifer Jones) for making my time at Texas A&M University a great experience. I also want to extend my gratitude to the National Institutes of Health, the Robert A. Welch Foundation, the Office of Naval Research, and the ARO for support.

Finally, thanks to my family (mother, father, and sisters) for their encouragement and to my husband and daughters for their patience and love.

TABLE OF CONTENTS

CHAPTER Page

LIST OF FIGURES

FIGURE Page

LIST OF TABLES

CHAPTER I

INTRODUCTION

Objective

Protein-ligand interactions are ubiquitous on cell membranes. Indeed, many important physiological functions primarily involve such protein-ligand interactions. These include cell signaling, pathogen binding, trafficking of lymphocytes, and the immune response (Figure 1.1).[1-4] Cell membranes' two-dimensional fluidity enables a great variety ligand-receptor binding processes to occur. Multivalent binding typically results in the reorganization of membrane-linked components. Many inhibitory drugs function by disrupting these interactions, especially by binding to proteins within the membrane.[5,6] Therefore, understanding the thermodynamics of binding as a function of membrane chemistry should provide critical insight into biological recognition and may lead to strategies for improved drug design such as the inhibition of viral entry or the termination of cancer metastasis. A proper understanding of ligand-receptor interactions will also be of great importance in the development and application of biosensors devices that exploit these interactions.

This dissertation follows the style of *the Journal of the American Chemical Society*.

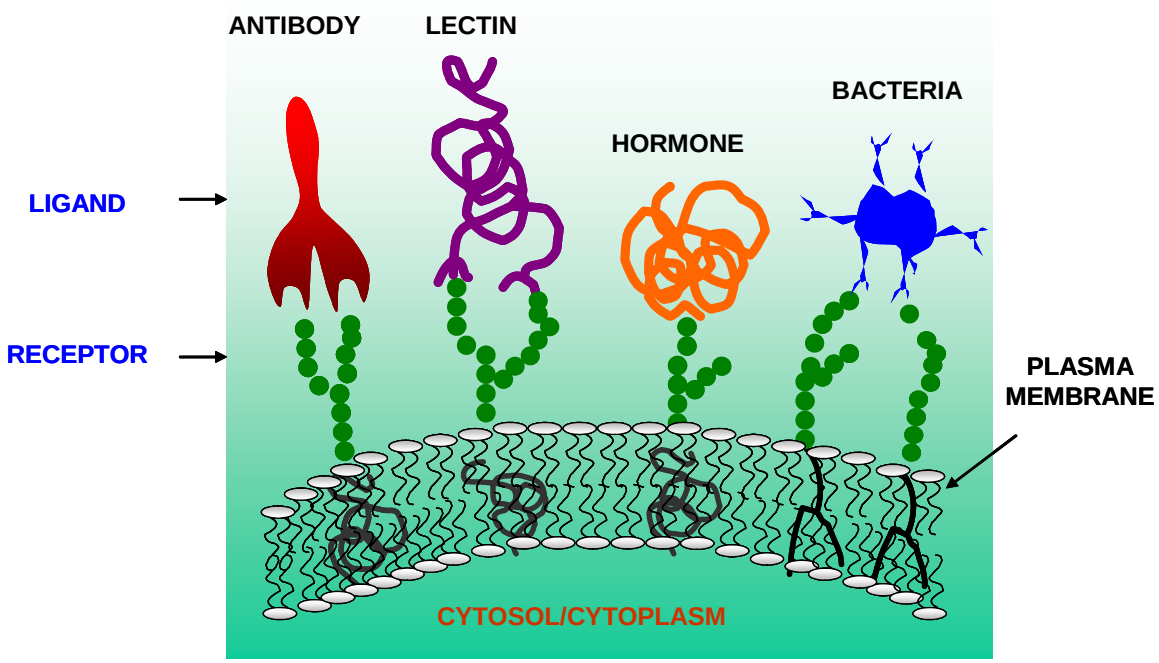

Figure 1.1. Schematic illustration of protein-ligand interactions on a cell membrane.

Techniques for monitoring ligand-receptor interactions are vital to a wide number of fields ranging from biotechnology to fundamental cell biology. Such measurements are often made by fluorescently labeling the proteins and nucleotides of interest. Indeed, fluorescent tags have become a ubiquitous tool for detecting protein-ligand interactions.[7] Labels can, however, interfere with the detection process and be extremely cumbersome to implement with real-time sensor devices.[8] This has been a major driving force behind the creation of assays that can detect biological analytes without labeling them (i.e. label-free detection). Methods for label-free detection include the use of liquid crystalline phase transitions,[9,10] colloidal particle imaging,[11] semiconductor nanowire conductivity,[12-14] quartz crystal microbalance (QCM) measurements,[15-17] and surface plasmon resonance (SPR) spectroscopy.[18-20] These techniques, however, are not always easy to employ, can give a nonlinear response to the analyte, require specialized equipment, and/or suffer from poor sensitivity in comparison with fluorescence-based measurements.[21]

We wish to develop a simple label free assay that could be run in imaging mode for multiplexed data collection while still retaining very high sensitivity. Moreover, the method should be simple to use and compatible with standard laboratory equipment such as a fluorescence microscope or plate reader. Thus, it should not require the purchase of an additional dedicated instrument or specialized assay platforms (e.g. metal coated chips). Specifically, we are interested in developing assays with the high sensitivity of fluorescence techniques, but without labeling the target analyte with a fluorophore. surface. These dyes should work as the sensor elements upon specific protein binding.

Instead, we are interested in directly embedding a fluorescent dyes onto a substrate. This could be achieved if the substrate-bound dye's fluorescence would be strongly enhanced by a specific binding event. Such an idea would therefore combine the best advantages of label-free detection with fluorescence measurements.

Up to 30 % of the open reading frames in an organism's genome encode for membrane proteins, yet these species remain strongly underrepresented in many state-of-the-art separation assays. A key aspect of our work is to move away from the agarose and acrylamide gels that are typically used in chromatographic processes. Instead, we employ a planar supported phospholipid bilayer (SLB) platform that allows proteins, including transmembrane species, to reside in a native-like environment while undergoing electrophoretic separation. In particular, we introduce lipid rafts into supported lipid bilayers as separation media. Using these rafts-containing bilayers as separation matrices, we wish to demonstrate the separation of two similar membrane-anchored lipid components by electrophoresis: 1,2-dipalmitoyl-*sn*-glycero-3-phosphoethanolamine-N-(cap biotinyl) (biotin-DPPE) and 1,2-dioleoyl-*sn*-glycero-3-phosphoethanolamine-N-(cap biotinyl) (biotin-DOPE).

Fluid-supported lipid bilayers

Planar supported bilayers are composed of the same lipid molecules found in the plasma membranes of living cells. Moreover, they possess the same two-dimensional fluidity as cell membranes,[22] and are capable of mimicking the lateral rearrangements that take place *in vivo* on the cell surface.[23] It is known that a thin water layer

(approximately 0.5-1.5 nm in thickness) generally resides between the lower leaflet of a supported bilayer and the underlying substrate (Figure 1.2). This enables individual lipid molecules to facilely translate along the surface.[24] Therefore, several ligand molecules can bind to a single protein with multiple binding sites simply by undergoing two-dimensional arrangements (Figure 1.3). Since a wide variety of lipid-conjugated ligands can be incorporated into the membrane, it is possible to study the effects on their specific chemistry and presentation on multivalent binding in a highly controlled manner. Results for several different hapten-antibody and ganglioside toxin interactions are provided below. The results demonstrate that ligand presentation is far more important than ligand density in determining the overall protein affinity for the membrane surface.

High-throughput microfluidic devices

Exploiting microfluidic devices for the quantitative investigation of multivalent ligand-receptor interactions in lipid membranes was first established by our laboratory.[25] Traditional binding measurements had previously been done using a standard flow cell geometry.[26] Such experiments usually required long periods of time to make sequential binding measurements as well as large sample volumes of precious protein solutions. Consequently, limited information about ligand-receptor interactions could be abstracted from a given set of measurements. By contrast, microfluidic platforms provided a high throughput/low sample volume approach to such measurements. Moreover, binding data at multiple protein concentrations can be collected simultaneously. Therefore, the methods often avoid several sources of noise associated with temporal variations in

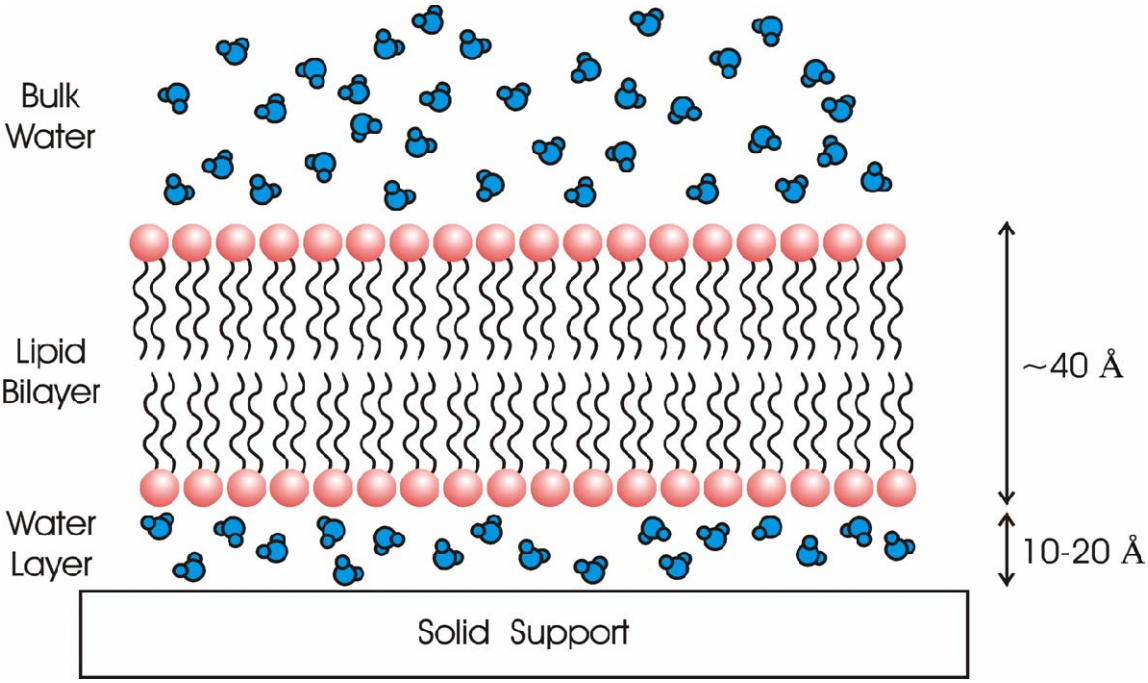

Figure 1.2. Schematic illustration of a supported lipid bilayer on a planar solid substrate. The underlying surface is hydrophilic and typically made of glass, quartz, and mica. Approximately 1-2 nm of water reside between the lower leaflet of the bilayer and the underlying substrate. Therefore, this model system is known to conserve many of the properties of native cell membranes such as a two dimensional fluidity.

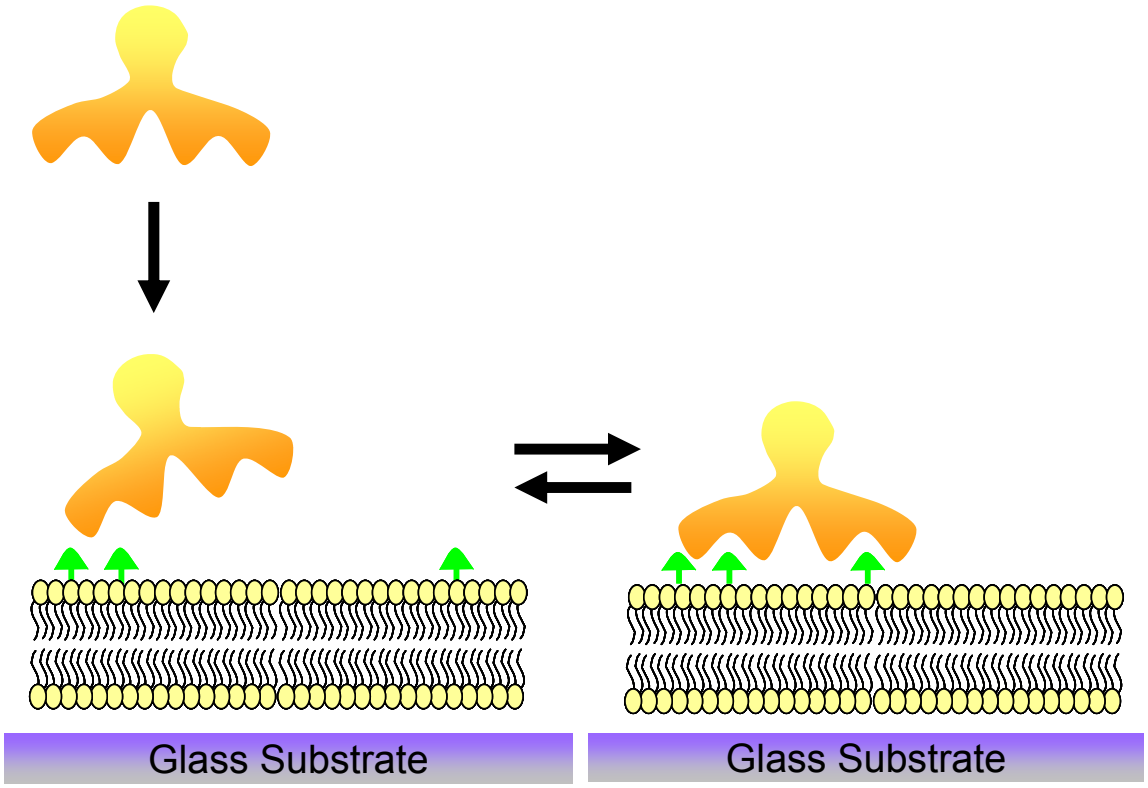

Figure 1.3. Schematic illustration of a fluid supported lipid bilayer facilitating a bivalent ligand-receptor binding event. The ligand (in green) undergoes lateral rearrangement within the fluid lipid bilayer to bind to an antibody (in orange) in two consecutive steps.

illumination intensities from an arc lamp source as well as detector drift.

The typical set-up employed in our laboratory for ligand-receptor binding studies is illustrated in Figure 1.4a. As can be seen, the heart of the device consists of a polydimethylsiloxane (PDMS)/glass multi-channel microfluidic device. The PDMS mold is patterned via standard soft lithographic techniques.[27] Lipids are coated on the walls and floor of this platform via the vesicle fusion method.[28] Next, a completed PDMS/glass device is situated on top of a dove prism. A drop of immersion oil is introduced between the device and the prism to allow total internal reflection fluorescence microscopy (TIRFM) measurements to be made.[29]

Dye-labeled protein solutions are then simultaneously flowed through each channel at varying concentrations. The evanescent field generated at the liquid/solid interface excites fluorescent molecules adjacent to the interface with high specificity (Figure 1.4b).[25,30,31] The amount of adsorbed protein within a given channel is found to be linearly proportional to the intensity of fluorescence [26] under the conditions which are employed. Additional contributions from labeled proteins in the near surface bulk volume can be subtracted away by performing control experiments with no ligands in the membrane.[32] A plot of fluorescence intensity vs. bulk protein concentration from a typical experiment is provide in Figure 1.4c. A line profile of these data can then be used to construct a standard binding isotherm from which a K_D values can be abstracted

(Figure 1.4d). Since the binding of proteins from aqueous solution at many concentrations is monitored simultaneously, it is possible to watch the entire binding curve evolve. Equilibrium is typically established more quickly at the highest protein concentrations. On the other hand, the system takes longer to reach equilibrium at lower bulk protein concentrations because of diffusion limits to the surface. Protein solution is constantly flowed through the device until the fluorescence signal from the entire TIRFM area remains unchanged. This can take several hours or more for pM concentrations of protein solution.

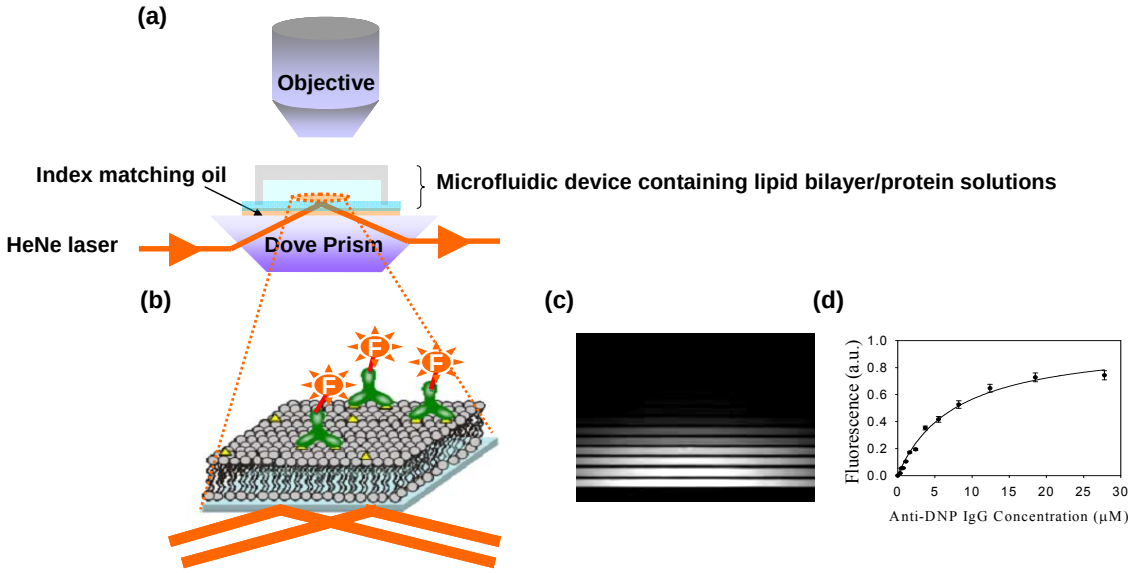

Figure 1.4. (a) Schematic of the experimental setup for performing ligand-receptor binding measurements in microfluidic devices. (b) Schematic representation of proteins adsorbed on the supported bilayer surface. (c) Total internal reflection fluorescence micrograph of a working device. (d) A one-shot binding curve obtained from the data in (c).

CHAPTER II

EXPERIMENTAL SECTION

Materials

Biotin-4-fluorescein (B4F), Texas Red DHPE, and Alexa Fluor-594 labeling kit was purchased from Invitrogen (Eugene, OR). ω-Hydroxyl α-amino polyethylene glycol was obtained from Jenkem Technology USA (Plano, TX). Affinity purified polyclonal anti-biotin IgG from goat (lot # 15501, Rockland, Gilbertsville, PA) and polyclonal anti-DNP IgG from goat (lot # A150-117A-1, Axxora, San Diego, CA) were used as received. Rabbit polyclonal anti-biotin antibody came from Rockland (Gilbertsville, PA). Cholera toxin B from *Vibrio cholerae* was purchased from Sigma-Aldrich (St. Louis, MO). Streptavidin was purchased form Rockland (Gilbertsville).

1-Palmitoyl-2-oleoyl-*sn*-glycero-3-phophocholine (POPC), 1, 2-dipalmitoyl-*sn* -glycero-3-phosphoethanolamine-N-(cap biotinyl) (sodium salt) (biotin-cap-PE or biotin-DPPE), 1, 2-dioleoyl-*sn* -glycero-3-phosphoethanolamine-N-(cap biotinyl) (sodium salt) (biotin-DOPE), 1,2-dioleoyl-*sn*-glycero-3-phosphocholine (DOPC), 1,2-dipalmitoyl-*sn*-glycero-3-phosphocholine (DPPC), ganglioside GM_1 (brain, ovine-ammonium salt), cholesterol, and 1,2-dipalmitoyl-*sn*-glycero-3-phosphoethanolamine-N-[6-[(2,4-dinitrophenyl)amino]c-aproyl] (DNP-cap-PE) were purchased from Avanti Polar Lipids (Alabaster, AL). 1,2 – dioleoyl – *sn* – glycerol - 3-phosphoethanolamine-N-[methoxy(poly(ethylene glycol)-5000)] (ammonium salt) (PEG^{5000}-PE),1,2-distearoly-*sn*-glycero-3-phosphoethanolamine-N-[methoxy(poly(ethylene glycol) - 2000)]

(ammonium salt) (PEG^{2000}-PE), 1,2-distearoyl-*sn*-glycero-3-phosphoethanolamine-N-[biotinyl(polyethylene glycol)-2000] (ammonium salt) (biotin-PEG^{2000}-PE), 1,2-dipalmitoyl-*sn*-glycero-3-phosphoethanolamine-N-(7-nitro-2-1,3-benzoxadiazol-4-yl) (ammonium salt) (NBD-PE), and 1,2-distearoyl-*sn*-glycero-3-phosphoethanolamine-N-[amino(polyethylene glycol)-2000] (ammonium salt) (NH_2-PEG^{2000}-PE) were also obtained from Avanti Polar Lipids. Three additional molecules needed for these studies, DNP (5-fluorescein) (D5F), DNP-PEG^{2000}-PE, and DNP-PEG^{2000} were not commercially available, but could be easily synthesized as described below.

Thin layer chromatography (TLC) was carried out using precoated plates made of silica gel with a pore size of 60 Å and a layer thickness of 250 μm (Silica Gel 60 F_{254}, EMD Chemicals Inc., Germany). Purified water was produced from a NANOpure Ultrapure Water System (18.2 MΩ·cm, Barnstead, Dubuque, IA). Glass coverslips (25 × 25 mm, No. 2, Corning Inc.) were used as solid supports for the bilayers. Polydimethylsiloxane (PDMS, Dow Corning Sylgard Silicone Elastomer-184) was obtained from Krayden, Inc (El Paso, TX). Sodium phosphates and NaCl were obtained from Sigma-Aldrich (St. Louis, MO). Ammonium fluoride (NH_4F) was obtained from Alfa Aesar (Ward Hill, MA) and hydrofluoric acid (HF) was purchased from EMD. Platinum wire with a diameter of 0.25 mm was purchased from Alfa Aesar. All chemicals were used as received without further purification.

Synthesis of small organic ligand molecules

Synthesis of DNP (5-fluorescein) (D5F). To prepare D5F, 5-carboxyfluorescein succinimidyl ester (7.1 mg in dimethyl sulfoxide (DMSO)) was slowly added to a solution of *N*-(2, 4-dinitrophenyl)-cadaverine hydrochloride (4.8 mg) in 4.87 mL of sodium bicarbonate buffer (100 mM, pH 8.3). It should be noted that this represents a molar ratio of 1.0 to 1.1. An orange product formed immediately. The reaction was allowed to proceed for 1 h at room temperature in the dark under constant stirring. The reaction mixture was concentrated to an oil on a rotary evaporator and then redissolved in a $CH_3CN/CH_3OH/H_2O$ mixture (5:4:1 by volume) for silica gel chromatography. The product-containing fraction was further purified by preparative reversed phase high-performance liquid chromatography (HPLC) and characterized by time of flight mass spectrometry (TOF-MS). The molecular mass was found to be 626.1 Da as expected.

Preparation of vesicles containing DNP-PEG^{2000}-PE. Small unilamellar vesicles (SUVs) composed of NH_2-PEG^{2000}-PE (1 mol %)/PEG^{2000}-PE (0, 4, or 9 mol %)/POPC (99, 95, or 90 mol %) as well as NH_2-PEG^{2000}-PE (5 mol %)/POPC (95 mol %) were mixed with an excess of 6-(2, 4-dinitrophenyl)aminohexanoic acid, succinimidyl ester (DNP-X, SE, Invitrogen, Eugene, OR) in phosphate buffered saline (PBS). DNP-X was only sparingly soluble in the PBS solution so 100 μL of DMSO was added to the 500 μL aqueous solution to improve solubility. This solution was stirred for 4 h at room temperature. It should be noted that the PBS solution consisted of 20 mM Na_2HPO_4 and 150 mM NaCl. The pH value was adjusted to 7.2 by the dropwise addition

of NaOH. Purified water from a NANOpure Ultrapure Water System (18.2 MΩ•cm, Barnstead, Dubuque, IA) was employed for making all solutions.

Product-containing SUVs were separated from unreacted DNP-X, SE by size exclusion chromatography using standard procedures.[33] The formation of DNP-PEG^{2000}-PE was confirmed by matrix assisted laser desorption ionization mass spectrometry (MALDI-MS). The molecular mass was found to be 3051.5 Da in H^+ mode. The unreacted NH_2-PEG^{2000}-PE peak at 2788.1 Da was also found. This is not surprising because half the NH_2-PEG^{2000}-PE was facing inside of the vesicles during the reaction and should not be available. In fact, approximately 50 mol % of the NH_2-PEG^{2000}-PE was not conjugated to DNP. Control experiments demonstrated that NH_2-PEG^{2000}-PE did not bind to anti-DNP antibodies in supported membrane formats.

The mol % of DNP-PEG^{2000}-PE in each SUV was determined by forming supported bilayers with these lipids in POPC and performing quantitative binding measurements by introducing a saturation concentration of fluorescently labeled IgG molecules into the bulk phase. Such data were then directly compared to analogous fluorescence intensity results obtained with DNP-cap-PE in POPC at known ligand concentration. These results confirmed that half of the NH_2-PEG^{2000}-PE in each vesicle was converted to DNP-PEG^{2000}-PE as expected.

Synthesis of DNP-PEG^{2000}. 6-(2,4-dinitrophenyl)aminohexanoic acid, succinimidyl ester (4.2 mg in DMSO) was slowly mixed with a solution of ω-hydroxyl α-amino polyethylene glycol (16 mg) in sodium bicarbonate buffer (100 mM, pH 8.3). The molar ratio was 1.2 to 1.0. The reaction was completed after 3 h under constant

stirring. A yellow solid product was purified by silica gel chromatography and then characterized by MALDI-MS. The molecular mass was found to be 2329. 6 Da in H^+ mode.

Preparation of small unilamellar vesicles (SUVs)

Lipids in the desired composition ratio were introduced into a glass vial in chloroform. The solvent was removed by passing a gentle stream of dry nitrogen over the solution. The resulting film was further dried under vacuum for 3 h. The film was then hydrated in a 10 mM phosphate buffered saline (PBS) solution containing 150 mM NaCl. After suspension of the lipid mixture, it was subjected to 10 freeze-thaw cycles and then extruded 10 times through two stacked polycarbonate membranes (Whatman) with 100 nm pores. The resulting SUVs prepared by this procedure were 70 ± 10 nm in diameter as determined by dynamic light scattering (Brookhaven Instruments 90Plus Particle Size Analyzer). The final concentration of the lipid solutions employed for vesicle fusion experiments was 0.5 mg/mL. The vesicles were kept at 4 °C before use.

A side-by-side comparison of the lipid composition from vesicles and the subsequently formed lipid bilayer was made to confirm that they had identical composition. This was done by MALDI-MS. The results showed that the two compositions in bulk were the same within experimental error. Additional controls were performed to compare the ratio of intensities of dye (Alexa Fluor 594)-labeled PEG lipids[33] and NBD-PE in surface adsorbed vesicles and SLBs. The relative intensity ratio of the two dyes was found to be similar. Thus, it was assumed herein that the

concentration of hapten in the upper leaflet of the bilayer was similar to its concentration in vesicles.

Fabrication of microfluidic devices

Seven or nine-channel microfluidic devices (130 μm wide, 15 μm deep, and separated by 160 μm spacing) were formed by conventional soft lithographic methods.[34] First, glass substrates (soda-lime glass slides, Corning) were spin-coated with photoresist (Shipley 1827) and then exposed to UV light through a Kodak technical pan film photomask containing the appropriate image. After the substrates were treated in developing solution and baked overnight at 120°C, they were immersed in a buffered oxide echant (BOE) to etch the glass. The BOE solution was prepared with a 1:6 ratio (v/v) of 48% HF (EMD Chemicals Inc., Germany) and aqueous NH_4F (200 g in 300 mL purified water, Alfa Aesar, Ward Hill, MA).[35] The remaining photoresist was removed with acetone. Next, a degassed mixture of Sylgard silicone elastomer-184 and a curing agent (10:1 ratio (v/v)) was poured over the patterned glass substrate. The liquid PDMS was cured in an oven at 70 °C for 1 h and then peeled off the glass substrate. This elastomeric mold and a freshly cleaned glass cover slip were placed into a 25 W oxygen plasma for 30 s and immediately brought into contact to form the PDMS/glass device. The glass slides used in these experiments were cleaned in a boiling solution of ICN 7X (Costa Mesa, CA) and purified water (1:4 ratio (v/v)) for 30 minutes, rinsed with copious amounts of purified water, and dried gently under a flow of nitrogen gas. Finally,

the glass substrates were annealed in a kiln at 450 °C for 5 h before introduction into the oxygen plasma.

Formation of supported lipid bilayers

SLBs were formed on the walls and floors of microchannels by the spontaneous fusion of SUVs.[36] To do this, 5 μL of an SUV solution were injected into each channel immediately after the formation of a PDMS/glass device. The solutions were incubated in the channels for 10 minutes and then rinsed away with pure PBS buffer to remove excess vesicles. All SLBs employed in these experiments were verified to be homogeneous down to the optical diffraction limit under fluorescence microscopy using a 40× objective. This was even the case for ternary lipid mixtures such as biotin-cap-PE/PEG^{5000}-PE/POPC.

Fluorescence anisotropy measurements

Solution binding assays were performed by single-point fluorescence anisotropy measurements (Koala spectrofluorometer, ISS Inc., Urbana-Champaign, IL). Data were abstracted according to established procedures.[37] Briefly, samples were excited with vertically polarized light at 490 nm with a slit width of 8 nm. Emission measurements were made with both vertically, I_{VV}, and horizontally, I_{VH}, polarized light. Note that the first subscript on the intensity term refers to the excitation polarization, while the second subscript refers to the emission polarization. The correction factor, G, was determined as described elsewhere.[38] The fluorescence anisotropy, r, was then calculated as follows:

$$r = \frac{I_{VV} - GI_{VH}}{I_{VV} + 2GI_{VH}} \quad \text{with} \quad G = \frac{I_{HV}}{I_{HH}}$$

Circulating water baths maintained the samples at a constant temperature (25.0 ± 0.1 ºC). Background fluorescence corrections for antibody solutions were performed as well as PBS blanks. In all cases the control sample intensities were found to be less than 2 % of the B4F and D5F intensities.

Total internal reflection fluorescence microscopy (TIRFM)

Binding measurements with labeled antibodies were performed inside microfluidic devices in combination with TIRFM.[39] Alexa Fluor-594 tags were conjugated to the IgG molecules molecules using an Invitrogen labeling kit by following standard procedures. The labeled antibody solutions at various concentrations were flowed through each microchannel until the bulk fluorescence intensity from the dye-labeled antibodies remained constant as judged by epifluorescence measurements. A 594 nm helium-neon laser beam (4 mW, Uniphase, Manteca, CA) was projected onto the sample with a line generator lens (BK7 for 30°, Edmund Optics, Barrington, NJ) for TIRFM measurements. This created a uniform intensity profile perpendicular to the direction of flow of the microfluidic channels. On the other hand, the intensity of the beam parallel to the long axis of the channels corresponded to a Gaussian profile. The glass substrates for the microfluidic devices were optically coupled to a dove prism with index matching immersion oil (type DF, Cargille Laboratories, Ceder Grove, NJ).

It should be noted that one important advantage of our microfluidic assays is that the binding data at all protein concentrations can be monitored simultaneously as a function of time. Therefore, one can monitor the binding curve's evolution. It is typically observed that the lowest concentration points take the longest time to achieve their ultimate values. It should be further noted that antibody binding is reversible, but requires the presence of soluble ligand in solution to compete the antibody off the surface in a reasonable amount of time. This has to do with rebinding effects that have been studied by Thompson and coworkers.[40-43]

Background subtraction measurements were performed by measuring the fluorescence intensity of antibodies above supported lipid membranes containing no hapten-conjugated lipids.[39]

Separation of Texas Red DHPE isomers

The two isomers of Texas Red DHPE were separated by using a slightly modified form of our previously published procedures.[44] Briefly, small spots of the ortho/para mixture were made on a TLC plate from a 1 mg/mL chloroform solution. Next, the spotted plate was placed into a development chamber and ethanol (AAPER Alcohol and Chemical Co., Shelbyville, KY) was used as the eluent. Two bands were formed, whereby the upper band was the para isomer and the lower band was the ortho isomer. Each band was recovered separately from the plate by carefully scraping the surface with a razor blade and re-suspending the dye/silica bead mixture in methanol. The silica was separated from the soluble organic material by filtration. Methanol could

then be removed by using a rotary pump and further drying the sample under vacuum on a Schlenk line. TLC was rerun with a small portion of the isolated sample to confirm the purity of each isomer.

pH titration and buffer preparation

10 mM PBS solutions containing 150 mM NaCl were prepared at pH values ranging from 4.0 to 10.2 by mixing appropriate amounts of Na_2HPO_4, NaH_2PO_4, or Na_3PO_4. These pH values were chosen to locate the pK_A value of *ortho*-Texas Red DHPE. The pH could be adjusted to the desired value by the dropwise addition of HCl or NaOH. The pH was measured with a standard glass electrode setup. Such absolute measurements had an error of ± 0.1 pH units associated with them. Changes in fluorescence, however, could be measured far more accurately. These changes in fluorescence intensity corresponded to relative shifts in interfacial pH as small as 0.002 pH units when a 40× objective was employed for making the measurements. Titration curves for the dye molecules in SLBs were obtained by systematically changing the pH of the bulk solution in a stepwise fashion. Fresh buffer was continuously flowed over the surface until no further changes in fluorescence intensity could be observed. The quality and fluidity of the supported bilayers as a function of pH was confirmed by fluorescence recovery after photobleaching (FRAP) measurements.[45] Fluorescent micrographs of SLBs were captured with a standard epifluorescence microscope setup (Nikon Eclipse E800).

The fluorescence titration curve of the Texas Red DHPE dye molecules was monitored in SLBs containing two narrow, parallel lines of bilayers with distinct dye chemistries. The first line contained 99.47 mol % POPC/0.50 mol % biotin-cap-PE/~0.03 mol % *ortho*-Texas Red DHPE. The second line was identical, but contained *para*-Texas Red DHPE instead of the *ortho* isomer. The surrounding lipid matrix was a 1:1:1 mixture of DOPC, DPPC, and cholesterol. This composition was chosen because diffusion of the dyes molecules from the narrow lines into the surrounding matrix was extremely slow. The two lines were formed sequentially by mechanically scratching the DOPC/DPPC/cholesterol bilayer and backfilling with the desired lipid mixture using the vesicle fusion method.

The titration curve for the Texas Red DHPE dye molecules in the presence of a saturated anti-biotin protein monolayer on a supported membrane surface was obtained with the same bilayer as described above. In this case, however, a saturation concentration of IgG (500 nM) was first introduced into the bulk solution. Moreover, all fluorescence measurements as a function of pH were performed in the presence of 500 nM bulk protein concentration to ensure that the surface remained saturated with protein.

All experiments presented herein were conducted with 150 mM NaCl. Additional control experiments were performed with varying concentrations of salts up to 300 mM. The results showed that fluorescence changes upon protein binding were not affected within experimental errors when moderately high salt concentrations were present. This is to be expected because the Debye length is below 1 nm so long as there is at least 100 mM NaCl in the buffer solution.[46]

Preparation of glass substrates

Glass coverslips (25×25 mm^2, #2, Corning) were cleaned in a boiling solution of ICN 7X (Costa Mesa, CA) and DI water (1: 4 (v/v)) for 30 minutes, rinsed with copious amounts of DI water, and dried with nitrogen gas before any additional treatments. A buffered oxide etchant (BOE) solution was prepared by 1:6 ratios (v/v) of 48 % HF: 200 g NH_4F in 300 mL DI water. **Baked glass substrate**: cleaned glass substrates were annealed in a kiln at 450 °C for 5 h to yield flat surfaces with a typical root mean square roughness (RMS) value of 0.31 nm over a 1 μm^2 area as determined by AFM. **HF-etched substrate**: baked glass substrates were gently wafted by hand in BOE solution for 5 or 10 minutes, washed in a 1M HCl solution for 1 minute, rinsed thoroughly with DI water, and dried under nitrogen gas. The RMS value of HF-etched substrate was found to be 0.41 nm by AFM. **Piranha-etched substrate**: glass substrates were cleaned for 5 minutes in a solution of 4:1 (v/v) concentrated sulfuric acid and 35 wt % hydrogen peroxide (Acros, NJ), rinsed with extensive amounts of DI water, and dried in a gentle stream of nitrogen. *(Caution: Piranha solution is extremely hazardous and must be handled with care).* All substrates were used immediately after treatment.

Formation of lipid rafts of varying size

Supported lipid bilayers were formed via a vesicle fusion method.[47] A drop of vesicle solution (150 μL) consisting of DOPC/DPPC/cholesterol (1:1:1) and Texas Red DHPE (0.03 mol %) were placed on the appropriately treated glass substrate. A polydimethylsiloxane (PDMS) mold was used to confine supported lipid bilayers on

glass substrates. The mold was made by cross-linking PDMS between two silanized glass microscope slides (50×75 mm^2, Corning) separated by a thin metal spacer between 200 and 400 μm thick. After cross-linking, a rectangular hole (1×2 cm^2) was cut out of the center of the thin elastomeric sheet using a razor blade. Vesicle solutions were allowed to warm to room temperature (22-25 °C) before use. Texas Red DHPE was incorporated into the membrane composition to visualize raft and non-raft regions after they were formed. The solution was confined to a rectangular area in the center of the substrate by a thin PDMS wall and incubated on the substrate for 10 minutes. Excess vesicles were rinsed away from the surface with copious amounts of DI water. **Large microrafts (11 μm)**: lipid bilayers formed on the HF-etched (10 minutes) substrate were heated at 50 °C for 2 h and slowly cooled back to room temperature. **Medium microrafts (7 μm):** lipid bilayers formed on the HF-etched (5 minutes) substrate were heated at 50 °C for 2 h and slowly cooled back to room temperature. **Small microrafts (2 μm):** lipid bilayers formed on the piranha-etched substrate were heated at 50 °C for 1 h followed by cooling to room temperature. **Nanorafts (98 nm):** lipid bilayers formed on the baked substrate were heated for 1 h and cooled down to room temperature. **Nanorafts (42 nm):** lipid bilayers formed on the baked substrate were heated for 25 minutes and cooled down to room temperature. **No observable rafts:** lipid bilayers were formed on the baked substrate and no heat treatment was applied. Raft and non-raft regions in supported bilayers were characterized by fluorescence microscopy and AFM.

Partition coefficients (K_{pi}) of molecules into rafts

To quantify the partitioning of two biotin lipids (biotin-DPPE and biotin-DOPE) between raft and non-raft regions, rafts of 7 μm size were formed by using the following lipid composition: DOPC/DPPC/cholesterol (1:1:1) containing biotin-DPPE (1 mol %) or biotin-DOPE (1 mol %), respectively. Raft and non-raft regions were then visualized by staining those lipids with Alexa Fluor 594-labeled streptavidin (0.5 μM). The intensities were corrected for dark counts and stray light by subtracting the average background intensity measured for bare glass. The average fluorescence intensities of areas corresponding to these regions were calculated from 16-bit digitized CCD fluorescence micrographs. The partition coefficient (K_{pi}) was defined as $K_{pi} = I_r/I_n$, where I_r and I_n were the background-corrected average fluorescence intensities measured in the raft and non-raft regions, respectively. The quantum efficiencies of the fluorophores attached to the probe molecules (Alexa Fluor-594 in this case) and the matrix lipid densities are assumed to be identical for both raft and non-raft regions.

Epifluorescence microscopy

An inverted epifluorescence Nikon Eclipse TE2000-U microscope with a 10× air objective (N.A. = 0.45) was used for FRAP studies. Laser radiation from a 2.5 W mixed gas Ar^+/K^+ laser (Stabilite 2018, Spectra Physics) was used to bleach a small spot (14 μm in diameter) in the supported bilayer sample.

Fluorescence imaging studies were performed with a Nikon Eclipse E800 fluorescence microscope (Tokyo, Japan) equipped with a MicroMax 1024 CCD camera

(Princeton Instruments), a Texas Red filter set (Chroma Technology, Bellows Falls, VT) and either a 4× air (N.A. = 0.13) or a 10× air (N.A. = 0.45) objective. An X-Cite 120 arc lamp (EXFO) was used as the light source for all experiments and all images were processed with MetaMorph software (Universal Imaging). Data acquisition for the limit of detection experiments was also performed in epifluorescence mode. In this case, a 40× oil immersion objective (N.A. = 1.30) was used to monitor the fluorescence intensity.

Atomic force microscopy (AFM)

AFM imaging of supported lipid bilayers containing nanorafts and no rafts was performed as previously described elsewhere.[34] The bilayer-coated glass in AFM liquid sample cell were mounted on a J-type scanner of a nanoscope IIIa Multimode SPM (Digital Instruments, Santa Barbara, CA) under ambient conditions. The experimental conditions of the bilayers were identical to those used in fluorescence microscopy. Height images were acquired in fluid contact mode at a scan rate of 2.0 Hz using oxide-sharpened DNP-S1 silicon nitride probes (spring constant: 0.06 N/m, Veeco Probes, Santa Barbara, CA). Rafts were identified from non-rafts when the feature height exceeded ~ 0.7-1.1 nm above the membrane background.[48] All AFM images shown in this paper are flattened raw data.

Bilayer electrophoresis

Matrix lipid bilayers containing rafts of varying size were prepared as described above. A line of bilayer substrate was then carefully removed from the matrix lipid bilayers using a piece of metal tweezers and washed away with copious amounts of DI water. This process was found not to cause any damage to the underlying substrate. Immediately following this step, 150 μL of vesicle solution containing the two biotin lipid mixtures (1 mol % biotin-DPPE and 1 mol % biotin-DOPE) were added into the aqueous phase above the surface. The vesicles fused to the bare portion of the substrate, creating a thin bilayer strip (~100 μm width) with the biotin lipid mixtures. After incubation for 5 minutes, the sample was thoroughly rinsed with DI water. The DI water was used to avoid excessive Joule heating. A 125V/cm potential (DC) was applied laterally across the bilayers by placing a platinum wire electrode on each side of the PDMS wall with a standard regulated power supply (TCR 300, Sorensen). The current was monitored with a digital multimeter (177 Microvolt DMM, Keithly). Currents of only a few microamps or less were maintained during the application of high electric field strength. Electrophoresis was performed for 30 minutes. Next, the electrophoretically separated biotin lipids were stained with Alexa Fluor 594-labeled streptavidin (0.5 μM) for 10 minutes. Excess proteins were washed away with DI water. Biotin lipids migrated toward the positive electrode as expected from their charge (-1). A microscope with a 4× objective (N.A. = 0.13) was used to maximize the field of view in the results.

CHAPTER III

IMPACT OF HAPTEN PRESENTATION ON ANTIBODY BINDING AT LIPID MEMBRANE INTERFACES*

Introduction

Interactions which occur between proteins and ligands are ubiquitous in biological recognition.[40,49-51] Many drug molecules function by disrupting these interactions, especially by binding to proteins at membrane interfaces.[52,53] Curiously, the equilibrium dissociation constants for drugs with membrane proteins *in vivo* are often only in the micromolar range.[54,55] This is the case despite the fact that many of these interactions are nanomolar or even picomolar when originally screened *in vitro* in the absence of a lipid bilayer. There is some evidence in the literature that the partitioning of drug molecules into lipid membranes occurs via lipophilic interactions.[54,56,57] It certainly is possible that such interactions as well as interactions with the cell's glycocalix are responsible for suppressing K_D values for drug molecules *in vivo*. Therefore, we wished to test the binding affinity of ligand-receptor interactions for model binding systems at membrane surfaces as well as in bulk solution to see if lipophilicity and steric effects could modulate the binding constants of simple antibody/antigen systems.

---

* Reproduced with permission from "Impact of Hapten Presentation on Antibody Binding at Lipid Membrane Interfaces" by Jung, H., Yang, T., Lasagna, M. D., Shi, J., Reinhart, G. D., and Cremer, P. S. 2008. ***Biophys. J.,*** 94, 3094-3103, Copyright 2008 by Elsevier.

The specific binding of antibodies with their target antigens at cell surfaces is a key step in immune response.[58,59] The recognition of membrane-conjugated haptens by free protein molecules is, in contrast to solution recognition, complicated by the presence of the cell membrane interface.[60] Previous studies have shown that binding between IgG molecules and antigens bound in the membrane depends upon the specific conditions of the experiment. For example, the McConnell group reported qualitative data which indicated that the binding of anti-DNP antibodies with DNP-conjugated lipid haptens was reduced above the chain-melting transition temperature of a lipid bilayers compared to the same system in the gel state.[61,62] The authors suggested that the DNP moieties can interact with the interior of the fluid lipid bilayers. Additionally, PEG-modified lipid membranes are believed to decrease the efficiency of the ligand-receptor recognition processes. Kim,[63] Moore,[64] and their coworkers have reported that the adhesion strength of ligand-protein interactions depends on the ligand accessibility within the PEG layer. Dori and coworkers demonstrated that cell adhesion to peptide ligands in a supported bilayers can be controlled by the addition of PEG-conjugated lipids to the membrane.[65] Such effects can be desirable. In fact, PEG-conjugated liposome surfaces have been shown to have long circulation times *in vivo*.[66,67] The extracellular PEG layer is generally believed to stabilize the liposome surface via steric repulsion effects.[68,69]

PEG moieties can also be used to enhance binding rather than inhibit it. For example, target molecules are often tethered to the terminal end of a PEG chain for site specific liposome drug delivery.[70-72] Similarly, ligands can be covalently linked to

flexible spacers or tethers on lipid bilayers. It is known that protein binding to ligands at surfaces via long, flexible polymer tethers can be more efficient than when the tether is very short.[73-75] Such tethers may serve to orient the ligands, which could aid in the efficacy of antibody binding depending on the relative hydrophobicity of the linker. In fact, DNP and trinitorphenyl (TNP) haptens with sufficiently short or long hydrophobic spacers are known to be less effective for antibody binding than those with intermediate chain lengths.[76,77] Ahlers,[78] Leckband,[60] and their coworkers have emphasized long, flexible, hydrophilic ethylene oxide linkers for improving hapten presentation at bilayer interfaces.

Herein, we report that hapten presentation for binding aqueous IgG antibodies can be systematically manipulated depending upon the ligand's lipophilicity, the presence of membrane-conjugated PEG in the membrane, and the use of PEG linkers to conjugate the hapten. Specifically, equilibrium dissociation constants for the biotin/anti-biotin and DNP/anti-DNP systems were examined in bulk solution and at model membrane surfaces. Solution binding constants were determined by fluorescence anisotropy measurements.[37,79,80] For surface binding assays, lipid membrane-coated microfluidic devices were employed in conjunction with total internal reflection fluorescence microscopy (TIRFM),[81] a method previously established in our lab.[82] Lipid-conjugated haptens were incorporated into the supported lipid bilayers (SLBs), which are well-known to show specific antibody binding and retain many of the properties of native cell membranes.[22] Such methods rapidly provide highly accurate thermodynamic information while consuming relatively low sample volumes.

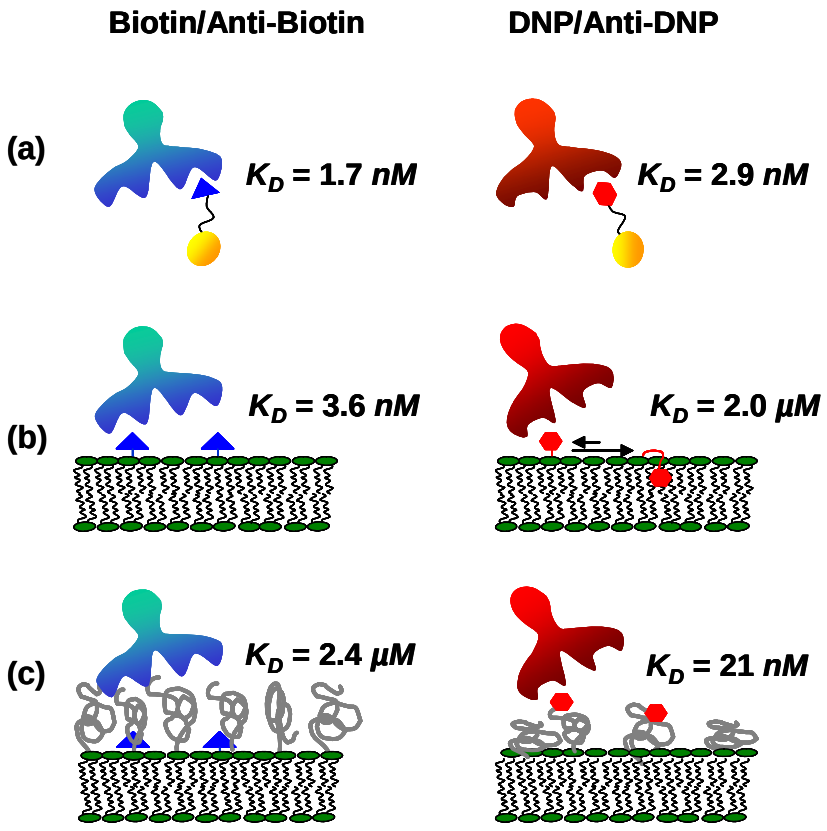

Figure 2.1. Schematic representation of antibody-hapten interactions. (a) Bulk solution. (b) Binding at phospholipid membrane surfaces. The hydrophilic biotin ligands are fully exposed to aqueous solution. By contrast, the lipophilic DNP ligands spend more time buried in the lipid phase. (c) Binding at PEG-coated surfaces. For the biotin case, the PEG lipopolymer screens the ligand. On the other hand, presenting the DNP ligand on the end of a PEG tether helps enhance binding.

The results of our experiments are summarized in Figure 2.1. It was found that anti-biotin and anti-DNP bind with their respective hapten moieties in bulk solution with nearly identical affinity (low nanomolar K_D values). At a lipid membrane interface, anti-biotin was still found to bind to lipid-conjugated biotin with very strong affinity. By contrast, the equilibrium dissociation constant was greatly weakened for anti-DNP binding to lipid-conjugated DNP on a supported lipid bilayer. This result can be explained in terms of the relative lipophilicity of DNP compared with biotin. Most of this lost affinity could be recovered by linking the DNP moiety to the end of a PEG^{2000}-conjugated lipid (see Figure 2.2 for structure). On the other hand, biotin/anti-biotin binding could be weakened to micromolar affinity by covering the biotin-presenting interface under a pegylated layer. These results clearly demonstrate that interfacial binding affinity can be manipulated over a wide range of binding affinities simply by altering the nature of ligand presentation.

Results

Binding in bulk solution. In a first set of experiments, binding constants for antibody-hapten interactions were measured in bulk by the fluorescence anisotropy technique. The fraction of bound hapten, f_B, was estimated as follows:[83]

$$f_B = \frac{r - r_F}{(r - r_F) + R(r_B - r)} \quad \text{with} \quad R = \frac{F_B}{F_F} \tag{2.1}$$

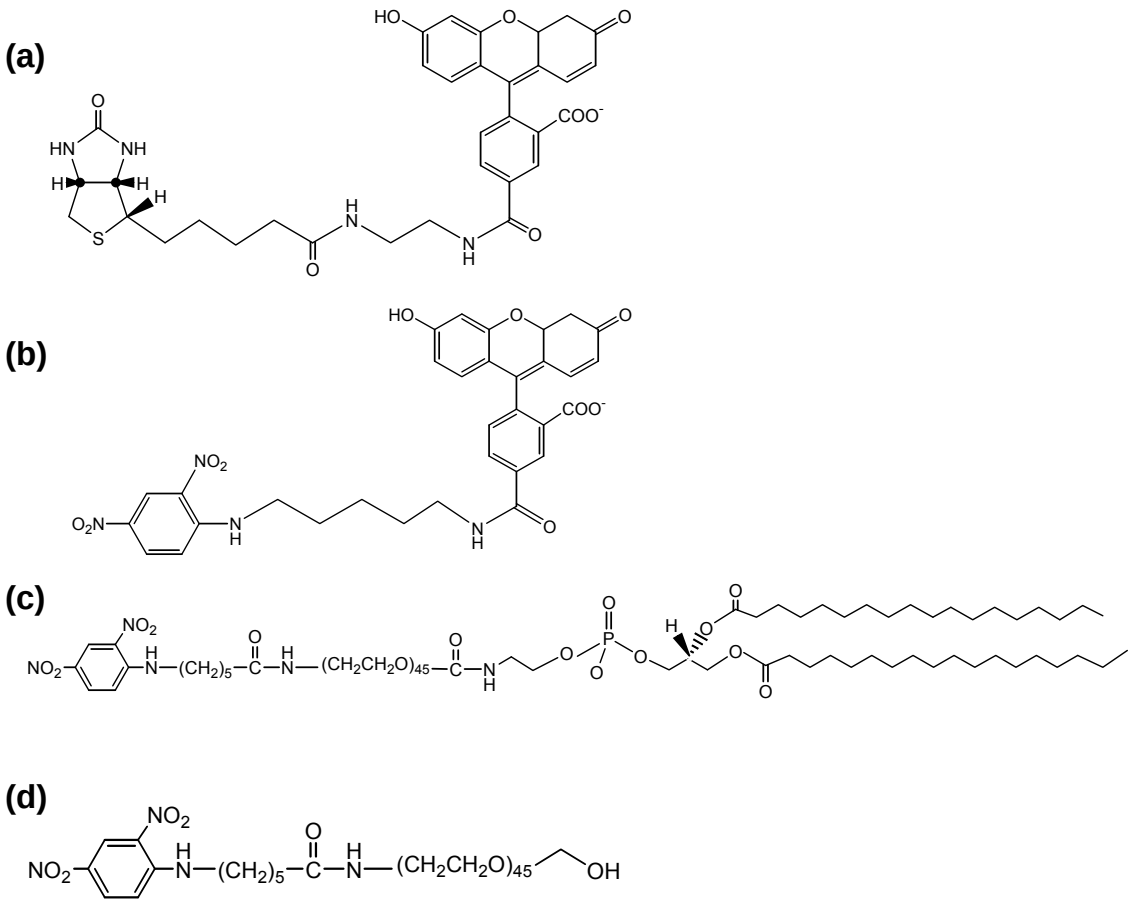

Figure 2.2. Structures of ligands. (a) B4F, (b) D5F, (c) DNP-PEG^{2000}-PE, and (d) DNP-PEG^{2000}. (a), (b), and (d) were used for solution binding measurements. (c) was used for surface binding measurements.

where r is the observed anisotropy. On the other hand, r_F and r_B are the anisotropies of the free and bound ligands, respectively. The parameter, R, was introduced to correct for changes in total fluorescence intensity upon complex formation.[84] Its value is determined by the ratio of the wavelength-integrated intensity of the free, F_F, and bound forms, F_B, of the dye-conjugated antigen as can be seen in Eq. 2.1. The absorption of the samples was matched and kept below 0.05 to avoid inner filter effects. The values of R were found to be 0.68 for biotin/anti-biotin and 2.3 for DNP/anti-DNP, respectively.

Experiments were performed with 1 nM of both B4F and D5F (see Figure 2.2 for structures). The antibody concentrations were varied. A Langmuir adsorption model was then employed to determine the apparent bulk equilibrium dissociation constant, $K_D(bulk)$:

$$K_D(bulk) = [P][L]/[PL] \tag{2.2}$$

where $[P]$, $[L]$, and $[PL]$ represent the concentrations of free antibody, free antigen, and the antibody-antigen complex, respectively. The total concentration of antigen in solution, $[L]_{tot}$, is:

$$[L]_{tot} = [L] + [PL] \tag{2.3}$$

From this relationship, the fractional binding, f_B, of ligand to the protein should be:

$$f_B = \frac{[PL]}{[L]_{tot}} = \frac{[P]}{K_D(bulk) + [P]} \tag{2.4}$$

The concentration of free antibody, $[P]$, was calculated by subtracting the bound antibody concentrations from the total protein concentration.[85]

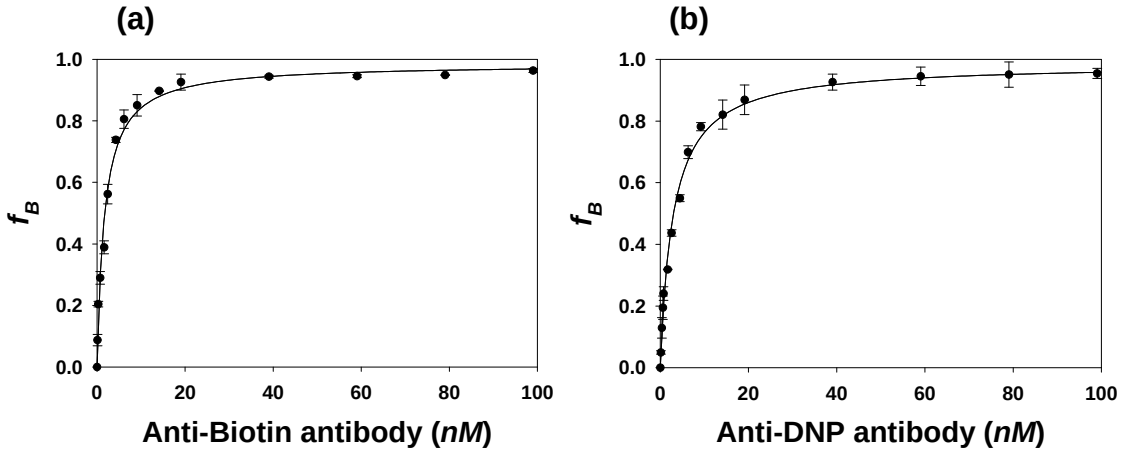

Figure 2.3. Binding isotherms in bulk solution obtained from fluorescence anisotropy measurements. (a) B4F binding with anti-biotin antibody. (b) D5F binding with anti-DNP antibody. Each data point represents the averaging of three measurements.

Non-specific binding as well as a correction term arising from the bound vs. free ligand concentrations was not taken into account. It should be noted, however, that the calculation is still considered to be valid in the present case because the ligand concentration (1 nM) did not exceed the measured $K_{D(bulk)}$ values.[86] Moreover, non-specific IgG adsorption on the walls of the sample holder (plastic cuvettes used) should be minimal because plastic rather than glass cuvettes were employed.[85,87]

Figure 2.3 shows the binding isotherms for the (a) biotin/anti-biotin and (b) DNP/anti-DNP binding pairs. The $K_{D(bulk)}$ values extracted from these data are equal to the concentration of free antibodies in solution at which half of the B4F and D5F molecules are bound to their respective antibodies. At 25 ºC, $K_{D(bulk)}$ was found to be 1.7 ± 0.2 nM for biotin/anti-biotin and 2.9 ± 0.1 nM for DNP/anti-DNP, respectively. These values are in good agreement with previous reports for each hapten/antibody system.[88,89] The present data are also consistent with the notion that the fluorescein and linker moieties do not significantly influence the $K_{D(bulk)}$ measurements. These results demonstrate that the intrinsic affinity of the two antibodies for their respective antigens in bulk solution is nearly identical.

Binding at lipid membrane surfaces. As with bulk binding data, a Langmuir adsorption model was employed for fitting data at membrane interfaces. The association of a free antibody in solution with an available membrane-bound hapten, L_s, led to the formation of a membrane-bound complex, PL_s, which could be characterized by a first dissociation constant, K_{D1}:

$$K_{D1}[PL]_S = [P][L]_S \tag{2.5}$$

A key difference between Eq. 2.2 and Eq. 2.5 is the presence of the subscript, *s*, which denotes the fact that the quantity is a two-dimensional concentration and has units of mol/dm^2. Moreover, the antibody is bivalent so that the PL_s complex can rearrange on the surface and bind to a second hapten to form PL_{2s}:

$$K_{D2}[PL_2]_S = [PL]_S[L]_S \tag{2.6}$$

where K_{D2} is the second dissociation constant. The total concentration of binding sites on the membrane surface, $[S]_s$, can be written as:[82]

$$[S]_S = \frac{1}{2}[L]_S + \frac{1}{2}[PL]_S + [PL_2]_S \tag{2.7}$$

It is assumed that the measured surface fluorescence is proportional to the surface protein concentration.[82] Therefore, the normalized surface fluorescence can be written in terms of a fractional surface coverage:

$$\frac{F([P])}{F([\infty])} = \frac{[PL]_s + [PL_2]_s}{[S]_s} = \frac{\alpha[P]}{K_D + [P]} \tag{2.8}$$

where $F([P])$ is the measured fluorescence intensity when the bulk concentration of labeled antibody is $[P]$. $F([\infty])$ is the fluorescence intensity when the membrane surface is completely saturated with dye-labeled antibodies. The parameter, α, is a constant that varies between 0.5 and 1.0 and reflects the degree of monovalent vs. bivalent antibody binding.[82] Formally, its value is dependent upon K_{D2} as:

$$\alpha = \frac{K_{D2} + [L]_S}{K_{D2} + 2[L]_S} \tag{2.9}$$

Finally, the value of the overall apparent equilibrium dissociation constant at the surface, K_D, depends upon both K_{D1} and K_{D2}:

$$K_D = \frac{K_{D1}K_{D2}}{K_{D2} + 2[L]_s} \tag{2.10}$$

Representative binding isotherms for anti-biotin and anti-DNP antibodies are shown in Figure 4. Measurements were made with phospholipid membranes consisting of 5 mol % of the ligand and 95 mol % POPC. It should be noted that the concentration of a free antibody in solution, [*P*], was equal to the applied concentration because the protein was continuously flowed through the microfluidic channels until equilibrium was established. The value of K_D for biotin/anti-biotin was 3.6 (±1.1) nM. By striking contrast, DNP/anti-DNP binding was much weaker. In this case K_D was 2.0 (±0.2) μM. Such a result is remarkable because these binding constants were nearly identical in bulk solution (Figure 2.3). At membrane interfaces, however, they differ by three orders of magnitude.

The K_D values obtained in Figure 2.4 should not be directly compared with the $K_{D(bulk)}$ values obtained in Figure 2.3. That is because the antibody can bind bivalently at the lipid interface and, therefore, the value of K_D is dependent upon both the first and second dissociation constants (Eq. 2.10).[59,82,90] Nevertheless, it should be pointed out that bivalent binding only enhances binding for an IgG by approximately one order of magnitude at high ligand density.[82] It should be noted that the phosphate groups of biotin-cap-PE and DNP-cap-PE were negatively charged (pK~3)[91] as well as the underlying glass support.[92] The antibodies employed in this study were also negatively charged at pH = 7.2.

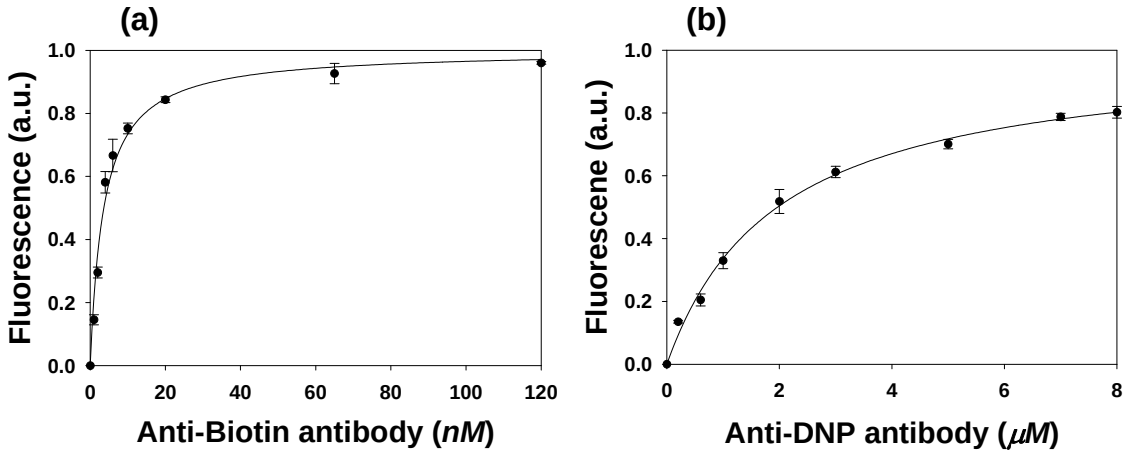

Figure 2.4. Surface binding isotherms. (a) anti-biotin antibody binding to 5 mol % biotin-cap-PE and (b) anti-DNP antibody binding to 5 mol % DNP-cap-PE. All data points represent the average of three independent runs. The solid lines represent the best fit of the data to simple Langmuir adsorption isotherms.

The protein charges were experimentally confirmed by pressure-mediated capillary electrophoresis,[93] which showed that the anti-DNP and anti-biotin antibodies bore the same charge. Therefore, electrostatic repulsion effects need to be considered. Indeed, Leckband and coworkers have previously reported that substrate electrostatics can affect the binding affinity at interfaces.[94] However, both the biotin-cap-PE and DNP-cap-PE supported bilayer systems on glass should bear the identical charge. Therefore, electrostatic repulsion probably cannot account for the three order of magnitude difference in binding for the DNP/anti-DNP system relative to the biotin/anti-biotin system. Indeed, the changes in binding affinity noted by Leckband and coworkers were rather modest (less than 1 order of magnitude) for relatively large changes in surface and protein charge density.

Binding at PEG-coated surfaces. SUVs consisting of biotin-cap-PE (1 mol %) and varying amounts of PEG^{5000}-PE in POPC were prepared as described in the experimental section. Surface binding measurements for the biotin/anti-biotin system were performed by the same procedures as described above. The abstracted K_D values vs. PEG concentration are plotted in Figure 2.5a. Without PEG in the membrane, K_D was 3.6 ± 0.2 *nM*, but weakened by an order of magnitude with just 0.2 mol % PEG^{5000}-PE. Moreover, the equilibrium dissociation constant continued to weaken as the density of lipopolymer increased. In fact, the K_D value was well into the micromolar range at the highest PEG^{5000}-PE concentration (1.5 mol % PEG^{5000}-PE). The greatest change in the K_D value occurred between 0.5 and 0.7 mol % lipopolymer. It is well known that PEG-PE undergoes a structural transition from the mushroom to brush state depending on its

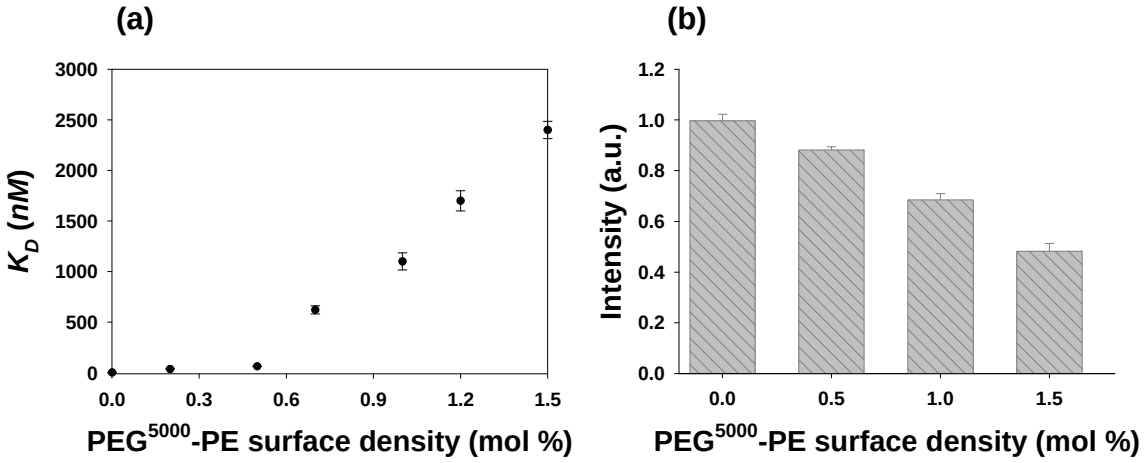

Figure 2.5. Binding between anti-biotin and biotin-cap-PE (1 mol %) at PEG polymer (M.W. 5000) coated lipid membrane surfaces. (a) Changes in K_D as a function of PEG^{5000}-PE concentration. All results are the average of three independent measurements. (b) Comparison of the relative fluorescence intensity from bound anti-biotin at saturation coverage ([IgG] = 20 μM) with varying surface densities of PEG^{5000}-PE.

surface density. Kuhl,[95] Bianco-Peled,[96] and their coworkers have directly measured the polymer thickness changes for this film using neutron reflectivity. PEG^{5000}-PE (M.W. = 5000 Da) polymers exhibit such transition around 0.5 mol % although it should be noted that this transition is rather broad.[97] These results appear to indicate that the brush conformation is more effective than the mushroom conformation at weakening the binding. Such a result is consistent with the notion that polymer molecules need to be pushed out of the way laterally in order for the IgG to bind at the lipid membrane surface, which was predicted by Szleifer[98] and Halperin.[99] This is energetically less costly in the more compressible mushroom state.

In addition to weakening the equilibrium dissociation constant, the amount of IgG which can be bound at saturation should also be affected by the density of lipopolymer in the membrane. To demonstrate this, membranes containing between 0 and 1.5 mol % PEG^{5000}-PE were challenged with a saturation concentration of anti-biotin (20 μM). The data clearly show that only about half as much IgG can be bound in the presence of 1.5 mol % PEG^{5000}-PE compared with the lipopolymer-free case (Figure 2.5b). This result can be understood on steric ground as there is only a finite amount of space for proteins to adsorb when PEG^{5000}-PE is also present.

It should be noted that increasing the PEG-PE concentration slightly increases the negative charge at the interface, although the change is very small compared with the large charge density on the underlying glass support.[92] Therefore, the relative increase in electrostatic repulsion between the surface and the negatively charged antibodies again needs to be considered. The results of Leckband and coworkers, however, clearly show

that that one needs much larger changes in charge density such as those caused by modulating pH to cause modest changes in affinity.[94] Moreover, Kenworthy and coworkers note that steric repulsion dominates over electrostatic effects for bilayers containing PEG^{2000}-PE and PEG^{5000}-PE.[100] Therefore, we judge the steric effects to be dominant in the present case.

Binding of anti-DNP to DNP presented on a PEG linker. In an effort to modulate the surface binding of DNP to anti-DNP, the hapten moieties were conjugated to the end of NH_2-PEG^{2000}-PE as described in the experimental section. SUVs were elaborated with ~1 mol % DNP-PEG^{2000}-PE and varying concentrations of PEG^{2000}-PE. The K_D value for the DNP-PEG^{2000}-PE/anti-DNP system was obtained by the same procedures described above. K_D was found to be 21 ± 10 nM for bilayers containing ~1 mol % DNP-PEG^{2000}-PE and no additional PEG^{2000}-PE (Figure 2.6a). This value is two orders of magnitude tighter than for DNP-cap-PE. To verify that this enhancement in K_D was only due to a change in ligand presentation, a solution binding constant measurement for DNP-PEG^{2000}/anti-DNP was made in bulk solution by fluorescence quenching.[59] The value of K_D was found to be 3.5 ± 0.6 *nM*, which is the same as the value obtained in Figure 3b within experimental error. This explicitly shows that the PEG linker does not significantly interfere with the equilibrium dissociation constant.

Additional control experiments were performed to test the effect of the DNP-PEG^{2000}-PE concentration on the binding affinity. The results showed that increasing the concentration of the PEG ligand up to five fold did not show any change in the measured

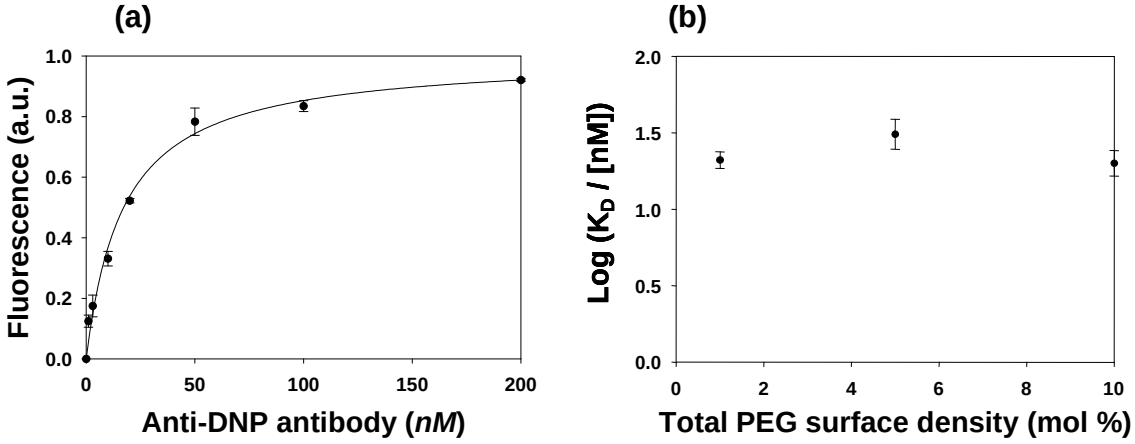

Figure 2.6. (a) Anti-DNP binding to ~1 mol % DNP-PEG^{2000}-PE in a POPC membrane. The solid line represents the best fit to simple Langmuir adsorption isotherms. (b) Plot of Log (K_D /[nM]) for ~1 mol % DNP-PEG^{2000}-PE with varying concentrations of PEG^{2000}-PE. All binding data were fit to simple Langmuir isotherm. The data points represent the average of three independent measurements.

K_D value. Therefore, this system appears to be insensitive to surface ligand density. To test the influence of DNP-PEG^{2000}-PE conformation on binding affinity, experiments were conducted by adding PEG^{2000}-PE to the membrane (up to 9 mol %), while holding the DNP-PEG^{2000}-PE concentration constant (Figure 2.6b). It is well known that increasing the polymer density causes these species to adopt a more brush-like conformation. [95,96,101,102] Again, no change was found in binding affinity, which indicates that the binding is also apparently insensitive to the conformation of the polymer-conjugated DNP ligand. A final control was performed by repeating these measurements using a biotin-PEG^{2000}-PE/anti-biotin system. Again, the K_D value was insensitive to ligand density and conformation (K_D = 3.6 ±1.0 *nM*). It should be noted that the biotin-PEG^{2000}-PE/anti-biotin K_D value is identical within experimental error to the one for the biotin-cap-PE/anti-biotin system.

Discussion and conclusion

Effect of hapten density vs. ligand presentation. The results in Figure 2.3-2.6 clearly demonstrate that protein-ligand interactions at lipid membrane interfaces can be strongly affected by ligand presentation. By contrast, our laboratory has previously reported results for the binding behavior of anti-DNP to DNP-cap-PE in a lipid bilayer as a function of ligand density.[82] In that case, the apparent equilibrium dissociation constant was found to be strengthened by only one order of magnitude as the ligand density was increased from 0.1 to 5.0 mol %. Moreover, we have recently investigated the pentavalent binding of cholera toxin to ganglioside GM_1 as a function of the

glycolipid density.[34] In that case the binding was actually weakened by slightly less than one order of magnitude by increasing the ligand density from 0.02 mol % GM_1 to 10 mol % GM_1. This decrease occurred because ganglioside-ganglioside interactions helped to inhibit ligand-protein binding. The present results suggest that ligand presentation is a more effective method than changes in ligand density for modulating the thermodynamic properties of interfacial binding.

Lipophilicity. The $K_{D(bulk)}$ values for biotin/anti-biotin and DNP/anti-DNP are virtually identical, yet the K_D values for the same binding pairs differed dramatically at the bilayer interface (Figure 2.3 and 2.4). We postulate that the relative lipophilicity of the hapten moieties is the origin of this dramatic difference. In fact, the octanol-water partition coefficient (log P) for DNP is 1.5,[103] but only 0.11 for biotin.[104] DNP is known to penetrate the outer membrane of mitochondria and associate with the inner membrane [105]. Balakrishnan and coworkers suggested that DNP haptens as well as other lipophilic molecules could bury themselves into lipid membranes via interactions with the aliphatic portions of the bilayer.[61] Qualitative results from their studies suggested that binding was stronger for gel phase membranes than for bilayers in the liquid crystalline phase. By contrast, the relatively hydrophilic biotin moiety should largely prefer the aqueous phase. In fact, the ureido moiety, (-NH-CO-NH-), of the 2-imidazolidone ring of biotin molecules undergoes hydrogen bonding interactions with biotin-binding proteins such as avidin and streptavidin.[106,107] Therefore, biotin should probably also bind to water in aqueous solution and thereby be more available for IgG binding.

Screening of anti-biotin by PEG density. PEG-coated lipid membrane surfaces can inhibit the binding of anti-biotin to surface conjugated hapten moieties (Fig. 5). Such an effect should be related to the types of mechanisms that are normally thought to be involved in the repulsive interaction between proteins and PEG films. In fact, the inhibition depends on PEG surface density just as is the case with resistance to biofouling.[108] Namely, increasing the surface density clearly shows a marked effect at the onset of the mushroom-to-brush transition. Szleifer[98,109] and Halperin[99] have provided theoretical insights into such steric repulsion mechanisms by modeling nonspecific protein adsorption. According to Szleifer, the protein must displace the polymer chains laterally in order to sit on the surface. This causes conformational entropy losses for the polymer molecules as well as protein-polymer repulsion, but is offset by protein-surface attractions.[110] Halperin predicted two possible nonspecific adsorption mechanisms for proteins on PEG films: an invasive mechanism at the surface and a compressive mechanism at the outer edge of the polymer brush. Small proteins penetrate the brush conformation with a relatively low free energy penalty (invasive mechanism). By contrast, large proteins indirectly contact the surface by compressing the polymer brush (compressive mechanism). Both Szleifer and Halperin predicted that the inhibition of protein adsorption is more pronounced with increasing PEG density rather than just increasing PEG chain length.[99,109,111] These theoretical models are in good agreement with our experimental results for specific ligand-receptor interactions.

Effect of a PEG linker on DNP presentation. Our results clearly demonstrate that the K_D value for the DNP/anti-DNP system can be strongly modulated by ligand

presentation using a PEG tether. We found that the K_D value for the DNP/anti-DNP system in the presence of the PEG tether was enhanced by two orders of magnitude at surfaces. These results seem to indicate that the solution properties in the environment immediately surrounding the ligand are critical. The use of a long hydrophilic polymer tether above the membrane almost certainly increases the partitioning of the DNP into the aqueous phase. As noted above, the octanol-water partition coefficient for DNP is 1.5.[103] This implies that DNP should favorably partition into the lipid bilayer compared to the adjacent aqueous phase. When a PEG linker is added, the DNP moiety instead must partition between the polymer film and the aqueous phase. Since the PEG layer is not as a hydrophobic as the lipid interface, a more equal partitioning should be expected. In fact, Slzeifer and coworker predicted that PEG polymer spacers increase the availability of the ligand, attenuate lateral repulsions, and, thereby, increase binding.[75]

It should be noted that the equilibrium dissociation constant for the DNP-PEG^{2000}-PE/anti-DNP system was still one order of magnitude weaker than for the biotin-PEG^{2000}/anti-biotin system at the membrane interface. Leckband and coworkers reported that PEG interacts at least modestly well with nonpolar, hydrophobic groups.[112,113] We, therefore, suggest that the DNP moiety probably still partitions to a significant extent into the hydrated PEG region in the present system.

Finally, it should be emphasized that the nanomolar equilibrium dissociation constant with the PEG tether represents the strongest binding for anti-DNP to a membrane-associated DNP for any method reported to date. By contrast, the introduction of cholesterol to a bilayer was found to only mildly enhance the binding

constant.[114] The use of a short PEG spacers such as $(EO)_2$ or $(EO)_4$ also had only a very modest effect.[115]

Glycocalix. The results presented herein lead to a central question. How does nature manipulate ligand presentation at a cell surface to regulate ligand-receptor binding? For example, does the cell's glycocalix, which consists of a network of glycoproteins, glycolipids, and related sugar moieties, serve to modulate or completely screen aqueous proteins based on their size? Moreover, are the equilibrium dissociation constants for drug molecules to membrane proteins really significantly altered from bulk values by the presence of the glycocalix? It is generally believed that the carbohydrate shell on the plasma membrane leads to the stabilization of the structure of the membrane via a variety of intra- and intermolecular physical interactions.[116] For drug molecules to bind target proteins, however, they must also often initially interact with membrane phospholipids.[117] Some investigations suggest that the composition of the lipid bilayer itself can affect drug sensitivity.[54,118] The results from the present experiments seem to be consistent with the notion that this sensitivity may arise from changes in the partitioning of the small molecule between the aqueous and lipid phases based upon hydrophobicity. This effect along with steric interactions may be the dominant properties attenuating apparent in vivo binding constants compared with those found in aqueous solution.

CHAPTER IV

DETECTING PROTEIN-LIGAND BINDING ON SUPPORTED BILAYERS BY LOCAL pH MODULATION*

Introduction

Ligand-receptor binding is ubiquitous in the chemical and biological sciences. Monitoring such interactions is often performed by fluorescently labeling the proteins or nucleotides of interest. In fact, fluorescent tags have become a standard tool for detecting biomolecules. Protein labeling can, however, interfere with detection measurements and be highly inconvenient to employ.[8] This has been a major driving force behind the development of assays that can detect biological analytes in a label-free fashion. To date, methods include the use of liquid crystalline phase transitions,[9,10] colloidal particle phase transitions,[11] nanoparticles,[119-121] semiconductor nanowire conductivity,[12-14] quartz crystal microbalance (QCM) measurements,[15-17] and surface plasmon resonance (SPR) spectroscopy[18]/imaging (SPRI).[122-124] Most of these techniques are performed at interfaces, but techniques to detect analytes in bulk solution are also being developed.[125,126]

Despite the tremendous progress in label-free detection, no technique to date offers the sensitivity and flexibility of fluorescence-based measurements. Indeed, fluorescence measurements can routinely by made down to the single molecule level

---

* Reproduced with permission from "Detecting Protein-Ligand Binding on Supported Bilayers by Local pH Modulation" by Jung, H., Robison, A. D., and Cremer, P. S. 2009. ***J. Am. Chem. Soc.,*** 131, 1006-1014 Copyright 2009 by American Chemical Society.

without the need for subsequent signal amplification steps. Moreover, fluorescent-based devices provide rapid readout and can be easily employed in an array-based format. Finally, with the exception of the protein tagging step itself, fluorescence spectroscopy/microscopy is relatively easy to perform. These advantages raise the question as to whether such techniques could be exploited for interfacial analyte detection without the need for tagging the target molecule. Instead, a fluorescent dye would be embedded onto the surface of a detection platform and employed as a universal sensing element for ligand/receptor binding in much the same way fluorescent dyes can be used to sense changes in pH or metal ion concentrations in bulk solution. Surprisingly, relatively little work has been performed until now to explore the use of fluorophores as an integral part of sensor platforms for detecting biomacromolecule binding. In one example, Swanson and co-workers exploited the aggregation of ligand-conjugated dye molecules to detect multivalent protein binding via a fluorescence quenching mechanism.[127,128] Also, Groves and co-workers exploited the change in the diffusion of membrane-bound fluorophores to detect protein binding.[129]

Herein, we employ pH sensitive fluorescent dye molecules to create biosensors that can be employed to monitor multivalent ligand-receptor interactions on supported lipid bilayers (SLBs). The dye fluoresces strongly in the protonated state, but becomes inactive upon deprotonation. The underlying physical principle for our detection method is based upon the idea that the binding of proteins to ligands at a surface will perturb the interfacial pH relative to the bulk value. Most proteins are negatively charged at physiological pH. Therefore, when these biomacromolecules adsorb on a surface, they

recruit hydronium ions with them and thereby lower the interfacial pH. Such local acidification is then reported by membrane-bound fluorophores near their titration point. A schematic diagram of this concept is shown in Figure 3.1. As can be seen, ligands (gray triangles) are incorporated into an SLB along with pH sensitive fluorescent dye molecules (shown in pink). The fluorophores are initially inactive. The binding of the negatively charged protein causes them to protonate and fluoresce strongly (shown in red). Precedence for this interfacial sensing idea is based upon the non-specific adsorption of charged polymers to oppositely charged surfaces to change the surface potential. For example, the pH sensitive fluorophore, hydroxycoumarin, has been employed to monitor the loading of DNA onto cationic liposomes in aqueous solution.[130,131] Moreover, it has been suggested that this concept might be applicable for other types of biomolecules, although no experiments were attempted.[132]

Most proteins possess a relatively modest charge per unit mass near physiological pH compared with DNA. Therefore, one needs to employ a very stable fluorophore as the pH sensitive interfacial detection element. Moreover, a suitable control system against which pH changes can be measured is also required. Texas Red DHPE is an ideal candidate for such measurements (Figure 3.2). Texas Red DHPE is made from Texas Red sulfonyl chloride via addition of the free amine from the head group of 1,2-dihexadecanoyl-*sn*-glycero-3-phosphoethanolamine (DHPE). Because Texas Red sulfonyl chloride consists of an *ortho* and a *para* isomer,[133] the conjugated lipid product is ultimately an isomeric mixture. The *ortho*-conjugated isomer fluoresces when the sulfonamide is protonated, but not when it is deprotonated (Figure 3.2a).[134]

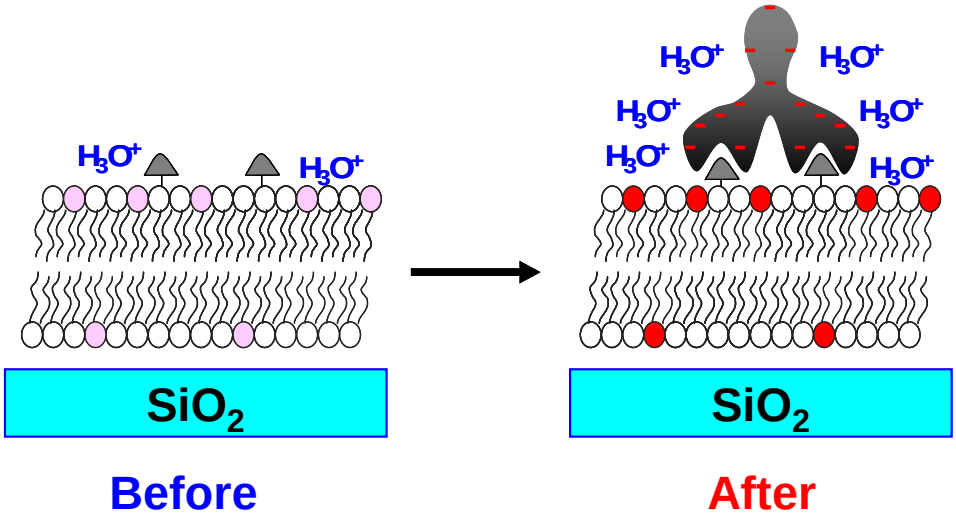

Figure 3.1. Schematic diagram illustrating the principle of a pH sensitive dye as a reporter for interfacial binding of negatively charged proteins. (Before) In the absence of proteins, the dye molecules fluoresce relatively weakly. (After) Upon specific protein binding, the dye molecules fluoresce strongly.

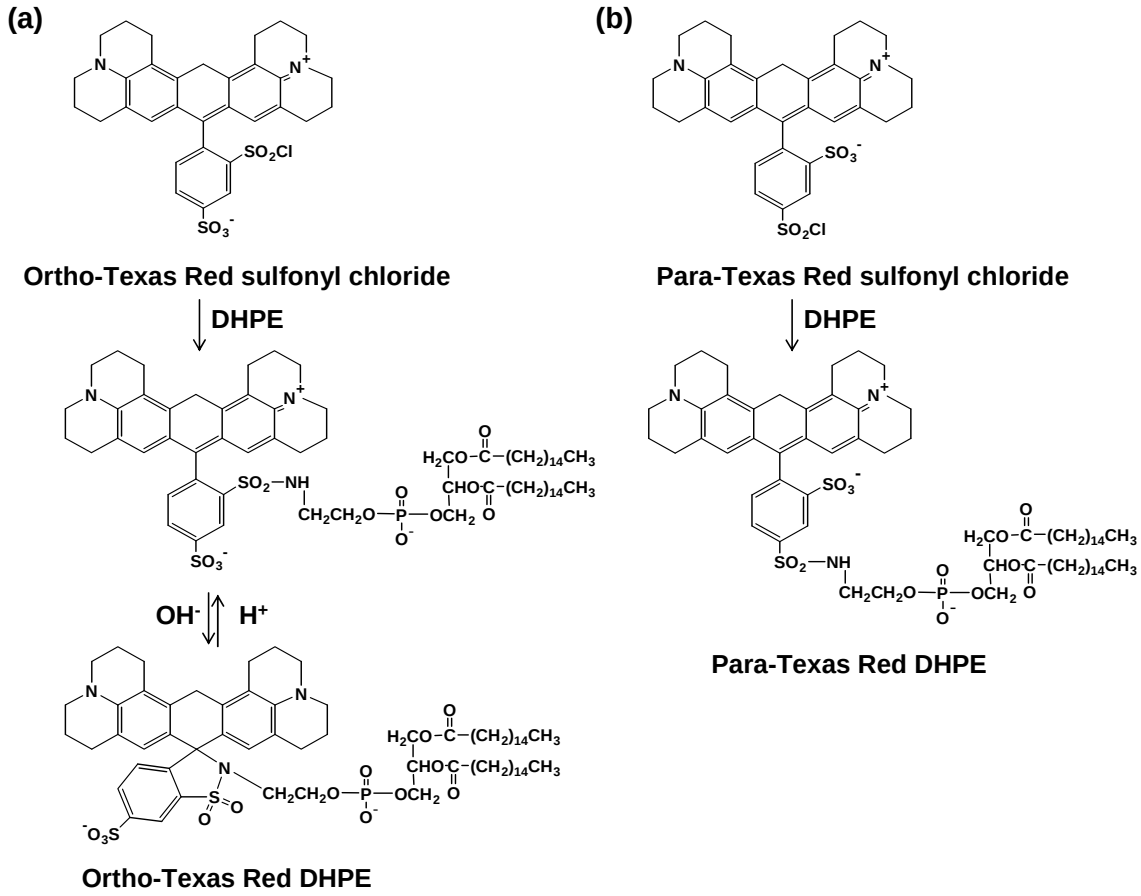

Figure 3.2. *Ortho*-and *para*-conjugated Texas Red DHPE. (a) The *ortho* and (b) *para* forms of Texas Red sulfonyl chloride are shown at the top. Both isomers can be conjugated to a primary amine (DHPE in this case). The *ortho* isomer forms a five membered ring upon deprotonation of the sulfonamide by attacking the xanthylium ring system (a). The *para* isomer does not undergo an equivalent reaction because of geometric constraints (b).

The process is perfectly reversible and it is possible to toggle back and forth between the two states by raising and lowering the pH.[133] This isomer is suitable for use as a pH sensor. By contrast, the *para* isomer of Texas Red DHPE is a pH insensitive dye and can be employed as a reference for determining relative changes in fluorescence intensity of the *ortho*-conjugated dye (Figure 3.2b). It should be noted that it is straightforward to separate the *ortho* and *para* isomers via thin layer chromatography (TLC) as well as by electrophoretic separation in a bilayer matrix.[44]

Herein, we demonstrate the use of *ortho*-conjugated Texas Red DHPE as a reporter of local pH modulation in supported lipid bilayers. The apparent pK_A of this molecule in an SLB containing 0.5 mol % biotin-cap-PE on glass was found to be 7.8 ± 0.1. The dye molecule could be used to generate a binding curve for the biotin/anti-biotin pair at the SLB interface. The equilibrium dissociation constant, K_D, was found to be 24 ± 5 nM. This value is in good agreement with measurements made by total internal reflection fluorescence microscopy (TIRFM) using dye-labeled proteins. Moreover, the limit of detection (LOD) for the antibody was ~350 fM at the 99 % confidence level. This is about 69,000 times smaller than the corresponding K_D value. In imaging mode, the assay could detect fewer than 400 IgG molecules in a single 4 × 4 binned pixel region. Thus, this assay compares extremely favorably with previously developed detection techniques.

Results

Titration curves for ortho-Texas Red DHPE. In a first set of experiments, the pH dependent responses of the *ortho*- and *para*-conjugated Texas Red dyes were investigated in supported POPC bilayers with 0.5 mol % biotin-cap-PE. Titration experiments were systematically performed by changing the pH of the bulk solution stepwise from pH 10.2 to 4.0. Bulk solutions at a given pH value were continuously flowed into the device until the fluorescence intensity remained constant. Fluorescence images at each pH value were then captured (Figure 3.3a). As can be seen, the intensity of the *para* band remained nearly unchanged, while the *ortho* band showed higher intensity at more acidic pH values. No evidence for hysteresis was observed by returning the pH back to 10.2 from 4.0 or even by cycling the pH several times. The normalized peak area of the *ortho* band relative to the *para* band as a function of pH is plotted in Figure 3.3b and an apparent pK_A value of 7.8 ± 0.1 can be abstracted from the data.

Next, we attempted to determine how fast *ortho*-Texas Red DHPE can respond to bulk pH changes. To do this, two separated bilayer strips were formed containing the *ortho* and *para* dyes, respectively. Time-sequence fluorescence images were obtained as the bulk pH was abruptly increased from 4.0 to 10.2. The fluorescence micrographs and line profiles as a function of time are shown in Figure 3.4. As can be seen, the fluorescence changed almost as abruptly as the pH could be raised (i.e. within a few seconds). Such a result is in agreement with the response of an *ortho*-conjugated sulforhodamine isomer in bulk aqueous solution, which can respond to pH changes on

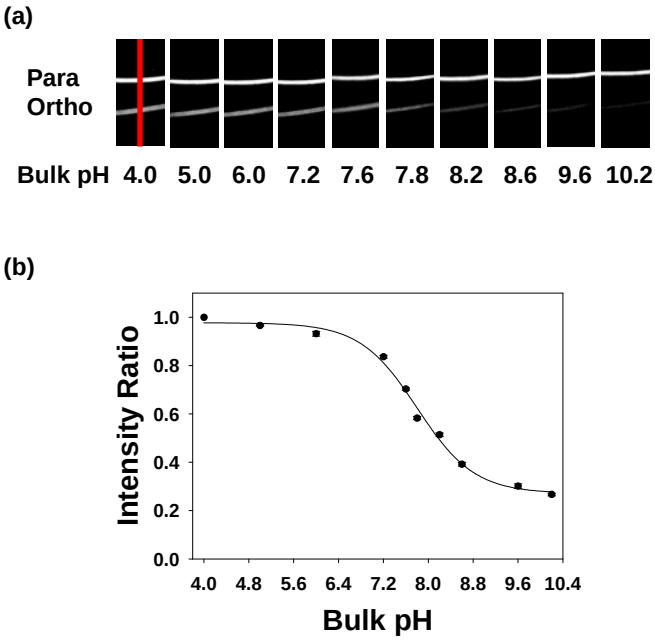

Figure 3.3. Titration curve for *ortho*-Texas Red DHPE. (a) Fluorescence images of supported POPC bilayers containing para and ortho-conjugated Texas Red DHPE in two adjacent bands. Each bilayer strip contained 0.5 mol % biotin-cap-PE and ~0.03 mol % of the respective fluorescent dye. The images were taken from pH 10.2 to pH 4.0. A 4× air objective was used to make these measurements. An example of the region from which intensity line profile data was abstracted is denoted with a red line in the first image. (b) Relative intensity for the *ortho*-conjugated isomer of Texas Red DHPE as a function of pH. The black circles represent individual fluorescence measurements and the solid line is a sigmoidal fit to the data. Error bars representing standard deviation measurements from three data sets are denoted on each data point. To obtain the y-axis, the intensity of the *ortho* band was divided by the intensity of the *para* band at each pH value. This ratio was normalized to 1.0 at pH 4.0. All intensity ratios are relative to this normalization.

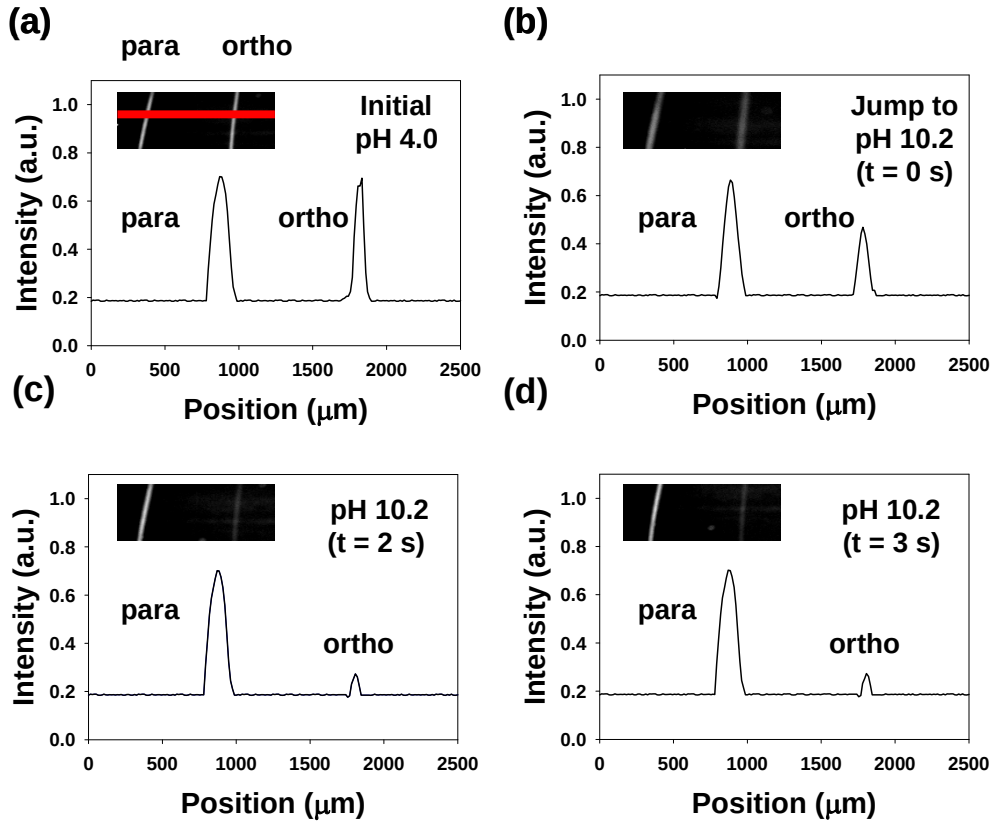

Figure 3.4. The time response of *ortho* and *para*-conjugated Texas Red DHPE bands in a supported bilayer to an abrupt jump in pH from 4.0 to 10.2. (a) pH originally set to 4.0, (b) buffer solution at pH 10.2 is flowed over the surface, (c) 2 s later, and (d) 3 s later. Both an epifluorescence image and a corresponding line profile are shown for each time period. An example of the region across which the line profile was taken is denoted with a red line in (a). A 4× air objective was used to make these measurements.

the millisecond time scale.[133] Moreover, it appears that Texas Red DHPE molecules in both leaflets of the bilayer are rapidly able to sense the pH jump.

Titration curve with a saturated protein layer. The *ortho*-Texas Red DHPE isomer should be an excellent reporter for small changes in the local pH brought about by the binding of proteins from bulk solution. To demonstrate this principle, the biotin/anti-biotin antibody binding pair was employed as a test system. First, two separated bilayer strips were formed as described above. Then, the surface was saturated with anti-biotin IgG by the introduction of a 500 nM protein solution over the surface for 10 minutes. All subsequent measurements were made by tuning the solution pH value, but keeping the bulk IgG concentration constant.[135] The results shown in Figure 3.5 reveal an apparent shift of ~0.35 pH units with respect to the results in Figure 3.3,[136] which were taken in the absence of bound proteins.

Binding curve for anti-biotin antibodies. To obtain the equilibrium dissociation constant for the biotin/anti-biotin system, POPC bilayers containing 0.5 mol % biotin-cap-PE and ~0.03 mol % *ortho*-Texas Red DHPE were coated on the inside walls and floors of a seven channel PDMS/glass microfluidic device. Experiments were run in all channels at a bulk pH of 8.2. Concentrations of antibodies ranging from 0 to 200 nM were flowed continuously through the individual channels until the fluorescence intensity from the surface-bound dyes remained constant. Epifluorescence images from

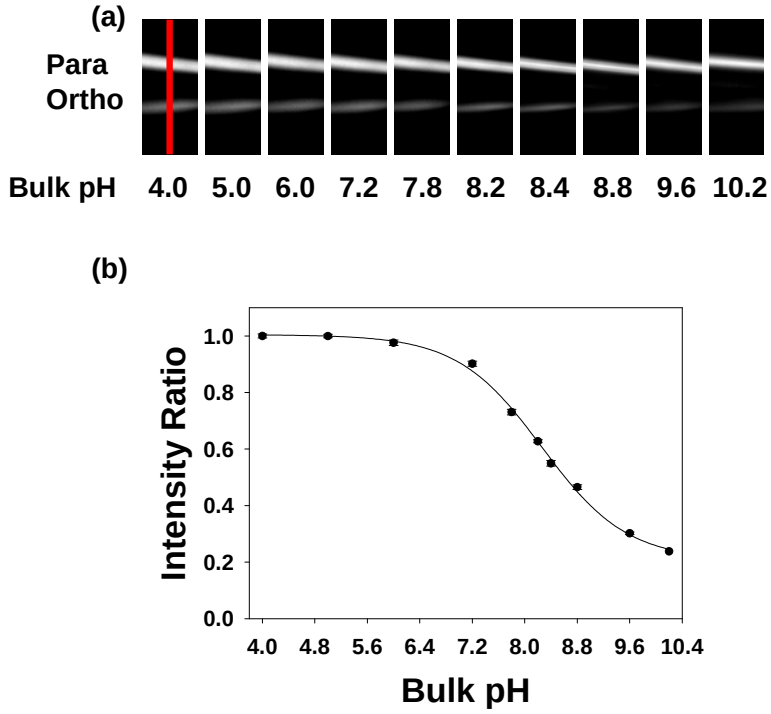

Figure 3.5. Titration curve with a saturated protein layer. (a) Epifluorescence images of para-Texas Red DHPE (upper) and ortho-Texas Red DHPE (lower) strips at different bulk solution pH values in the presence of a saturation concentration of anti-biotin. (b) Relative intensity ratio for *ortho*-Texas Red DHPE as a function of pH. The black circles represent fluorescence measurements and the solid line is a sigmoidal fit to the data (R^2 = 0.99). To obtain the y-axis, the intensity of the *ortho* band was divided by that of the para band at each pH value and the value at pH 4.0 was set to 1.0. All other intensity ratios are relative to this value. Error bars representing standard deviation measurements from three data sets are denoted on each data point. A 10× air objective was used to make these measurements. The red line across the first image in (a) denotes an example of the region from which intensity line profile data were abstracted.

the device used in these experiments are shown in Figure 3.6a. As can be seen, weaker and uniform fluorescence intensity was observed in all channels before the addition of protein. After the IgG molecules were introduced, however, the fluorescence intensity was strengthened in accordance with the bulk concentration of the antibodies.

Line profiles taken from the images (blue and red lines in Figure 3.6a) are plotted in Figure 3.6b. As can be seen, the fluorescence intensity after the introduction of the protein molecules increased and then leveled-off as the protein concentration was increased. It should be noted that the fluorescence intensity from the *ortho*-Texas Red DHPE was enhanced after protein binding by 1.4 times at the highest two bulk protein concentrations. Based on the curve in Figure 3.3b, the initial fluorescence intensity was 42 % of the maximum value and ended at 60 % of the maximum value upon protein binding. It should be noted that this interfacial pH shift occurred in the regime where the fluorescence intensity varied nearly linearly with pH (Figure 3.3b).

The normalized increase in fluorescence intensity as a function of bulk antibody concentration from Figure 3.6b is plotted as a function of bulk protein concentration in Figure 3.6c. Specifically, the y-axis plots the change in fluorescence intensity (ΔF) relative to the maximum change in fluorescence intensity when a saturation concentration of protein is present (ΔF_{max}). In order to extract the apparent equilibrium dissociation constant (K_D), the biotin/anti-biotin binding curves were fit to a simple Langmuir isotherm binding model (eq 1):

$$\Delta F = \Delta F_{\max} \times \frac{[P]}{K_D + [P]} \tag{3.1}$$

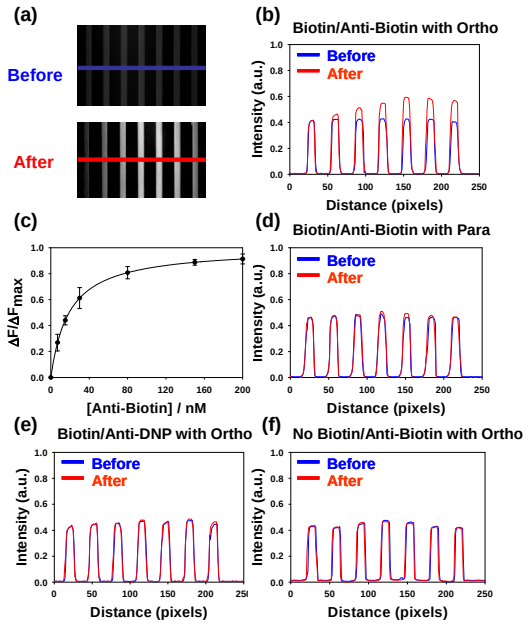

Figure 3.6. pH sensor-based binding assays. (a) Epifluorescence images of a bilayer coated microfluidic device before and after the introduction of unlabeled anti-biotin antibodies. The concentration of protein in the bulk solution was increased from left to right. The blue and red lines represent the regions used to obtain the line profiles shown in (b). (c) A plot of normalized fluorescence intensity ($\Delta F/\Delta F_{max}$) vs. bulk protein concentration. The solid line represents the best fit to a Langmuir isotherm. (d) Experimental line profiles for the same conditions shown in (b), but with *para*-Texas Red DHPE in the membrane instead of *ortho*. (e) Experimental line profiles for the same conditions shown in (b), but with anti-DNP antibodies. (f) Experimental line profiles for the same conditions as in (b), but in the absence of biotin-cap-PE. A 4× air objective was used to make all measurements. It should be noted that each data point in (c) represents the average of three measurements and the error bars are standard deviations from those measurements.

where [*P*] is the bulk antibody concentration. The fit to the curve for the data in Figure 3.6c yields $K_D = 24 \pm 5$ nM.

The biotin/anti-biotin binding experiments were repeated under a nearly identical set of conditions, but using *para*-Texas Red DHPE instead of ortho. The fluorescence line profiles both before and after antibody binding are shown in Figure 3.6d. As can be seen, little if any change in fluorescence intensity occurred under these conditions. Several additional control experiments were also performed. For example, anti-DNP antibodies, which are not specific for biotin, were used instead of the anti-biotin antibodies. Also, experiments were performed with anti-biotin antibodies and ortho-Texas Red DHPE, but without any biotin-cap-PE in the membrane. In both of these cases, the fluorescence intensities from the microchannels remained unchanged within experimental error upon the introduction of protein (Figure 3.6e & 3.6f, respectively). Such results are consistent with both high ligand-receptor specificity as well as relatively low levels of non-specific protein adsorption to the surface.

Next, classical antibody binding experiments were performed using anti-biotin antibodies labeled with Alexa Fluor-594 dye (Figure 3.7). Binding measurements were made by total internal reflection fluorescence microscopy (TIRFM)[137] as described previously.[36] In this case the supported membranes contained 99.5 mol % POPC and 0.5 mol % biotin-cap-PE. These experiments yielded a K_D value of 32 ± 7 nM. Therefore, the classical label and pH modulation assays gave nearly identical results within experimental error. Moreover, both values correlated well with previously reported values for biotin/anti-biotin interactions on supported membranes.[138]

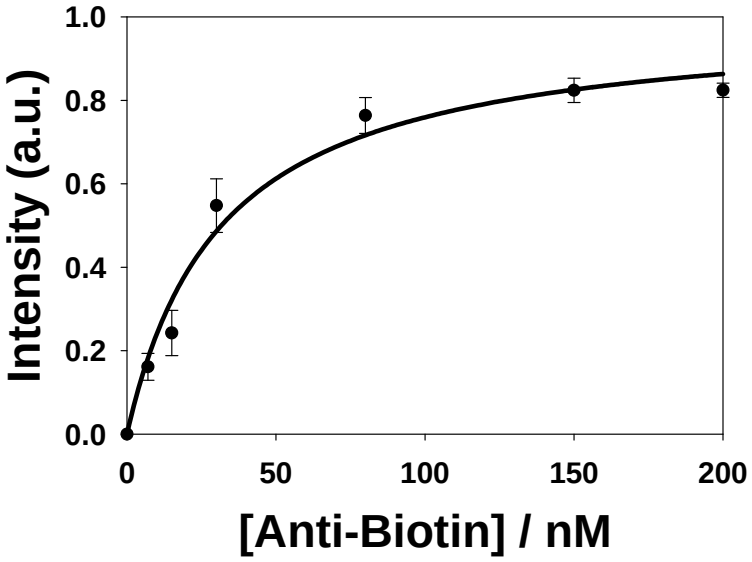

Figure 3.7. Plot of TIRFM intensity vs. bulk protein concentration for the labeled anti-biotin/biotin binding system. Each data point represents the average of three measurements and the error bars are standard deviations from those measurements. The solid curve through the data is the best fit to a Langmuir isotherm.

The similarities between the classical and pH modulation measurements as well as the associated control experiments are strong evidence for the reliability of the new assay. Specifically, the change of fluorescence intensity in the pH modulation assay appears to correlate linearly with the interfacial antibody concentration under the conditions of these measurements. Moreover, it should be noted that this assay is far easier to perform than its protein labeled counterpart. In fact, the classical binding assay requires that the antibodies be conjugated with fluorescent dye molecules and that free dye be subsequently separated from the labeled antibodies by running the mixture down a size exclusion column. Once the labeled antibodies are introduced into the microchannels, the fluorescence assay must discriminate between antibodies bound to the surface and those in the bulk solution above it. As noted above, this was done in the present case by TIRFM, a surface specific technique that requires a laser beam to be introduced to the sample past the angle of total internal refection.[139] By contrast, the pH modulation assay can be run in standard epifluorescence mode because the pH sensitive dye molecules are already located at the interface within the supported bilayer. Of course, no modification of the antibodies is needed to do these experiments.

Limit of detection (LOD) measurements. In a final set of experiments, we wished to determine the LOD value for this pH sensor assay by two different metrics. First, the CCD camera was used in imaging mode to determine the fewest number of IgG molecules that could be sensed. In that case 4 × 4 pixel binning was employed, which corresponds to a 1.7 μm^2 area at the lipid bilayer interface. Second, the experiments were repeated with 200 × 200 pixel binning to determine the lowest number

density of IgG molecules where could be detected. The camera contains a 1024 × 1024 pixel array.

To perform 4 × 4 binning experiments, supported bilayers were made from POPC lipids doped with 0.5 mol% biotin-cap-PE and ~0.03 mol% *ortho*-Texas Red DHPE. Concentrations of anti-biotin IgG ranging from 0 to 100 pM were introduced into the bulk solution. Line profiles both before and after the introduction of the protein are shown in Figure 3.8. As can be seen, the fluorescence intensity remained essentially unchanged when 0 pM anti-biotin was added (pure PBS buffer flowed for 60 min), but changed by ~8 % when 100 pM anti-biotin was added. It should be noted, that intensity changes were linear with concentration between 0 and 100 pM antibody as shown in Figure 3.8f (red circles). The slope of the line and its corresponding R^2 value is provided as an inset in the figure.

Error analysis of the intensity profiles revealed that the averaged fluorescence intensity over a given channel was stable to within ± 0.2 % over a 1 h time period. This gives an LOD value of ~8 pM if the limit of detection is defined as 2.58 times the experimental error. It should be noted that this definition of LOD was chosen because it represents the 99 % confidence limit for these measurements.[140] Control experiments with para-Texas Red DHPE under the same conditions showed that little if any change in fluorescence intensity occurred when the antibody was introduced (Figure 3.8f, black circles). Additional control experiments were performed with anti-DNP as well as without any biotin-cap-PE in the membrane (data not shown). No observable change in fluorescence intensity occurred.

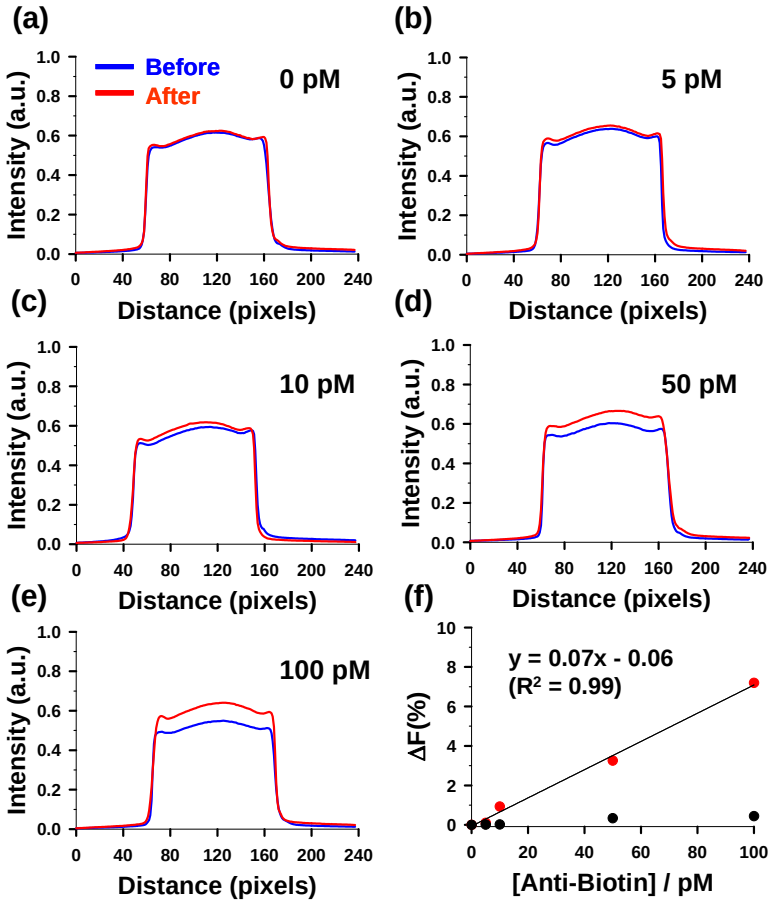

Figure 3.8. LOD results for 4 × 4 pixel binning. (a)-(e) Intensity line profiles across single microfluidic channels as various concentrations of anti-biotin antibodies were introduced to the bulk solution. The experiments were conducted at a bulk pH of 7.8 in 10 mM PBS with 150 mM NaCl. (f) A plot of the change in the fluorescence intensity of the *ortho*-Texas Red DHPE, ΔF(%), vs. bulk protein concentration (red circles). A control experiment was also performed with *para*-Texas Red DHPE in the membrane under otherwise identical conditions (black circles).

Next, the LOD was determined using 200 × 200 pixel binning. This dimension, which represents a 65 μm × 65 μm region of the liquid/solid interface, was chosen because it corresponds well to the width of an individual microfluidic channel. The experimental conditions were identical to those used above except for that pH was 8.2 for this experiments. Concentrations of anti-biotin ranging from 0 to 1.5 pM were introduced into the bulk solution. In this case, single data point intensities were recorded as a function of time (Figure 3.9a to 3.9e). Approximately 50 data points were obtained for each sample region over the course of 400 sec both before and after the introduction of protein. This was done to improve the signal-to-noise of the experiment. As can be seen, the fluorescence intensity remained stable to within ± 0.3 %. The data at each antibody concentration were averaged and plotted in Figure 3.9f (red circles). The LOD value was found to be ~350 fM at the 99 % confidence limit.

Discussion and conclusion

We have developed a novel pH sensitive assay for monitoring ligand/receptor binding at lipid membrane interfaces. The method should be quite general since most biomacromolecules in solution bear a net charge. Specifically, we found a shift of ~0.35 pH units occurred upon saturation binding of IgG to a lipid membrane with 0.5 mol% lipid-conjugated haptens compared to the case of no bound proteins. Such a result is in

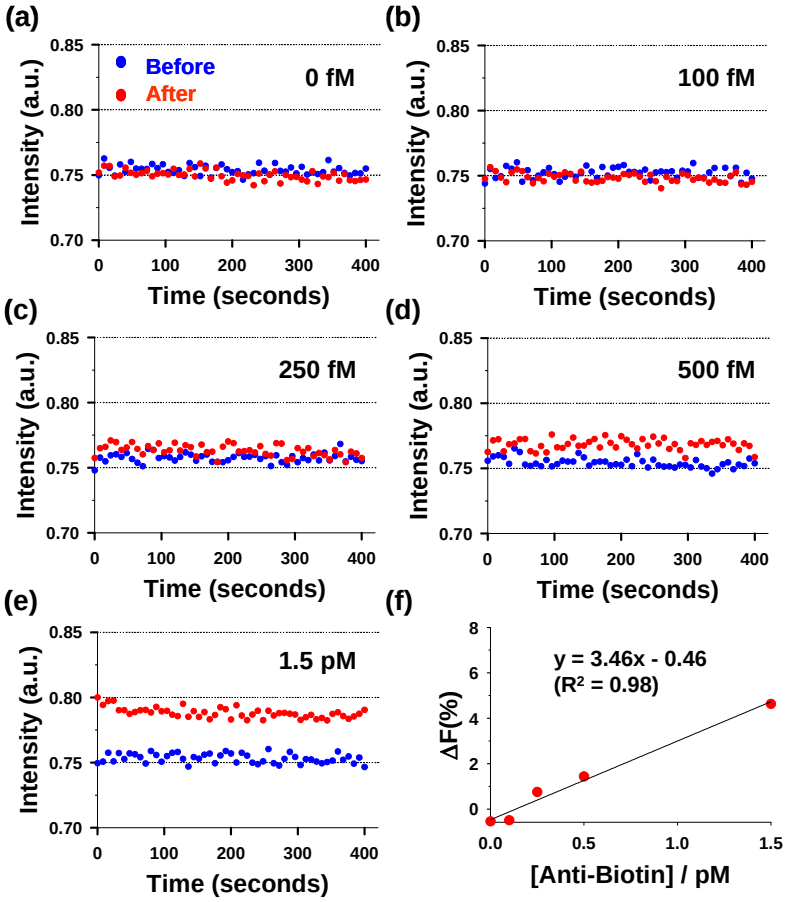

Figure 3.9. LOD results for 200 × 200 binned pixel regions. (a)-(e) Single point fluorescent intensity measurements as a function of time both before and after the introduction of various concentrations of anti-biotin. (f) A plot of fluorescence intensity for ortho-Texas Red DHPE, ΔF(%), vs. bulk protein concentration (red circles). The slope of the line and its corresponding R^2 value are provided in the figure.

agreement with the notion that increasing the density of negative charge at the interface recruits counterions (especially hydronium ions). In fact, Fromherz has suggested that changes in membrane potential can affect the interfacial concentration of hydronium ions and thereby shift the local pH.[141] Also, Latour and co-workers demonstrated that deprotonated COOH-terminated self-assembled monolayers (SAMs) attract hydronium ions to the interface, thus resulting in a decrease of the local pH value.[142] Changes in interfacial charge density, therefore, should lead to corresponding shifts in the apparent pK_A values of titratable surface groups relative to their values in bulk solution.[131] This makes the titration of fluorescent dye molecules useful for sensor development. How useful this phenomenon can be for assay development ultimately depends upon its sensitivity.

Sensitivity limits for biosensor platforms are often reported in the literature in terms of the minimum bulk analyte concentration that can be detected.[143] However, the LOD is usually strongly correlated to the strength of a given ligand/receptor binding event. For example, a typical antibody/antigen interaction might have a K_D value of 25 nM, while a tighter protein/ligand interaction could be K_D = ~1 pM. A heterogeneous detection assay (i.e. detection of the analyte by binding to a surface from solution) might have a detection limit of 250 pM for the former, but 10 fM for the latter. In reality, these apparently different bulk detection limit values may actually represent similar number densities of proteins at the interface because each LOD value would be 1 % of K_D. Therefore, the number of proteins at the interface which can be detected may represent a more intrinsic measure of the LOD value for a particular assay platform.

In the studies described in Figure 8, we employed 0.5 mol % biotin-cap-PE and used 4 × 4 pixel binning of our CCD camera with a 40× oil immersion objective for detection. This corresponds to a 1.7 μm^2 surface area at the liquid/solid interface for each binned pixel region. The area per lipid molecule in the membrane is known to be ~0.7 nm^2/lipid.[144] By assuming that biotin-cap-PE is roughly the same size as the lipids, 0.5 mol% of this molecule translates to ~7 × 10^3 ligands/μm^2 on the upper bilayer leaflet. The intensity change at 500 nM IgG is ~150 times greater than that observed at the LOD (~8 pM). Therefore, the number density of proteins at the interface should be ~150 times less than the saturated value. This results in a detection limit of ~380 IgG molecules if one assumes a 2:1 binding ratio between the antibody and the antigen.[139] Such a non-optimized result is within a few orders of magnitude of single molecule measurements. This result corresponds to a surface density of 56 pg/mm^2. This surface density LOD value can be substantially improved by binning together a larger number of pixels while making the binding measurements. Although one loses the ability to obtain a surface image, the signal to noise ratio should roughly improve with the square root of pixels employed. Additional improvements can be obtained by time averaging. The data for 200 × 200 pixel binning are provided in Figure 3.9. Such data represents an antibody surface density of ~2 pg/mm^2. Moreover, the 350 fM LOD is a factor of ~69,000 lower than the K_D value of 24 nM, although one is no longer sensing just a few hundred IgG molecules. It should be possible to sense even lower number densities of proteins by binning an even larger number of pixels together. Indeed, simultaneous sensing over a 1 mm^2 area should reduce the number density detection limit by yet another order of

magnitude. In that case, however, the ability to perform multiplex detection is completely eliminated.

Currently, surface plasmon resonance (SPR) is one of the most commonly employed label-free assays for monitoring ligand/protein binding at an interface. Direct comparisons between assays can sometimes be problematic. Therefore, we will limit this discussion to antibody/antigen binding measurements. In that case, SPR platforms in a Kretschmann configuration[145] gave rise to an LOD of ~3 pM for a system with a K_D value of ~4 nM.[18] For the present assay, we achieved a detection limit significantly better than that (~350 fM out of 24 nM). Of course, the sensitivity limits for SPR and SPRI can be vastly improved by secondary amplification steps.[120,146,147] By analogy, LOD from the current pH modulation assay could also be substantially enhanced by subsequent amplification procedures after antibody binding.

It should be noted that the pH modulation platform developed here should be highly versatile. Binding measurements were made on two dimensionally fluid lipid bilayers because these systems are laterally mobile and should allow the same type of multivalent protein binding to take place as occurs *in vivo* on a cell surface.[24] Moreover, supported lipid bilayer platforms are highly resistant to non-specific protein adsorption.[148] Nevertheless, this sensing concept could be expanded to any liquid/solid interface that contains substrate-conjugated ligands and pH sensitive fluorophores. It should also be capable of measuring nearly any protein-ligand binding event provided that the incoming macromolecule possesses a net charge and therefore changes the

interfacial pH. As another demonstration of the universality of this method, the binding of cholera toxin B to ganglioside GM_1 is provided in Figure 3.10.

In conclusion, a simple detection method based on pH sensitive dyes was developed. Specifically, ortho-conjugated Texas Red DHPE incorporated in supported phospholipids bilayers was used as an interfacial pH sensor. Such sensors have inherently excellent limits of detection and are relatively easy to use. Moreover, the method is fully compatible with multiplexed detection. Therefore, it could potentially be used in high throughput screening applications.

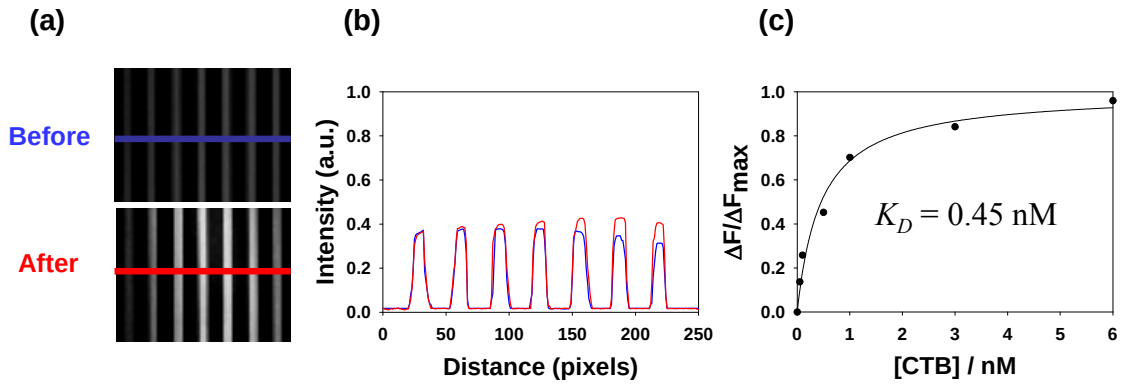

Figure 3.10. Binding constant measurements for cholera toxin B to GM_1 in POPC/*ortho*-Texas Red DHPE membranes. The experimental conditions were identical to those for the biotin/anti-biotin binding pair, but contained 0.5 mol % GM_1 instead of biotin-cap-PE. Moreover, the measurements were made at a bulk pH value of 8.2 (a) Epifluorescence images of the seven channel device before and after the introduction of the toxin. (b) Fluorescence line profiles from (a). (c) Fluorescence changes vs. bulk protein concentration. The binding curve was fit to a simple Langmuir isotherm as shown in Eq. 1 of the main text. The abstracted dissociation constant was K_D = 0.45 nM. This value is in excellent agreement with literature data obtained by fluorescently tagging cholera toxin B.[34]

CHAPTER V

BILAYER ELECTROPHORESIS USING LIPID RAFTS

Introduction

Separation and purification of membrane components such as lipids and transmembrane proteins is a challenging task. Conventional purification methods include extraction with detergents, centrifugation at high speeds, column chromatography and gel electrophoresis. These processing conditions can often deteriorate native structures of lipids and proteins and result in unwanted loss of materials.

Recently, our laboratory and other groups demonstrated a new electrophoresis method using solid supported lipid bilayers as a separation media for membrane-anchored components or bilayer electrophoresis.[149,150] Solid supported lipid bilayers are known to conserve many of the properties of native cell membranes including two dimensional fluidity.[24] It is generally believed that a thin water layer (approximately 0.5-1.5 nm in thickness) residing between the lower leaflet of the bilayer and the underlying solid support allows lipid bilayers to facilely move within the plane of the surface.[24] Bilayer electrophoresis is an attractive alternative to gel electrophoresis because it is run in native-like environments without further exposing the analytes of interest to harsh chemicals. A variety of solid supports can be used, from silica surfaces including mica, quartz, and glass to chemically functionalized surfaces such as gold, titanium oxide, and PDMS.[151] So far, several membrane components have been electrophoretically manipulated in solid supported lipid bilayers: charged lipids,[152,153] tethered vesicles,[154]

and glycosylphosphatidylinisotol (GPI)-linked proteins.[155] Recently, Boxer and coworkers reported the use of polymer-supported membranes to electrically manipulate recombinant proteins.[156] Electro-separation of membrane components using lipid environments provides an additional advantage: the separation can be simply tuned by modulating the lipid chemistry. For example, the presence of cholesterol in the bilayers reduced band broadening and improved band resolution during the separation process compared with the case in the absence of cholesterol.[149]

Rafts, domains enriched in sphingomyelin, saturated lipids, and cholesterol in cell membranes,[157,158] have attracted interest as they are thought to be involved in many important biological functions such as cell signaling,[159] protein sorting,[12,13] and membrane trafficking.[160] Their physical state is considered to be a liquid-ordered phase, while is distinct from the non-rafts are in a liquid-disordered phase. The partition equilibrium of membrane components between rafts and non-rafts is of particular interest. Lipid-anchored proteins are thought to be sorted using the partitioning properties of their anchor.[160] Indeed, a number of proteins in plasma membranes are modified with one or more lipid groups directly linked to the polypeptide backbone, suggesting that the lipid-modified sequences may influence the partitioning of proteins into rafts or related structures such as caveolae.[161] For instance, GPI- or saturated lipid-anchored proteins preferentially partition into rafts. In contrast, proteins anchored by unsaturated lipids are excluded from the raft regions[161], although this equilibrium is difficult to quantify in real biological systems due to the complexity of such systems.

Rafts have been previously formed using equal molar ratios of 1,2-dioleoyl-*sn*-glycero-3-phosphocholine (DOPC), 1,2-dipalmitoyl-*sn*-glycero-3-phosphocholine (DPPC), and cholesterol in model membranes. The phase diagram for this particular ternary mixture has been described in giant unilamellar vesicles (GUVs) studies.[162] However, unlike GUVs, formation of rafts on solid supported lipid bilayers is reportedly sensitive to solid surface treatments and the thermal history of the bilayers.[151,163,164] For instance, Hovis and coworker formed circular rafts of micrometer size by treating the glass substrates with piranha.[151]

Here we demonstrate electrophoresis of membrane-anchored components by using rafts-containing lipid bilayers on solid support as a matrix. The size of rafts was varied from the micrometer to the nanometer range by employing different surface treatments including Hovis and coworker's method. Large micrometer size rafts (large microrafts) could be obtained with HF-etched glass substrates where bilayers were then heated and slowly cooled down to room temperature. Small micrometer size rafts (small microrafts) were formed using methods developed by Hovis and coworkers.[151] Nanometer size rafts (nanorafts) were formed by controlling thermal history of bilayers on non-treated glass substrates. Raft and non-raft regions on solid supported lipid bilayers were characterized by fluorescence microscopy and nanorafts were further investigated using atomic force microscopy (AFM).[165,166] These solid supported lipid bilayers containing rafts of various size were then used as a matrix to electrophoretically separate membrane-anchored lipid mixtures. The two lipid components employed, biotin-DPPE and biotin-DOPE, contain the same head group, but differ in the structure

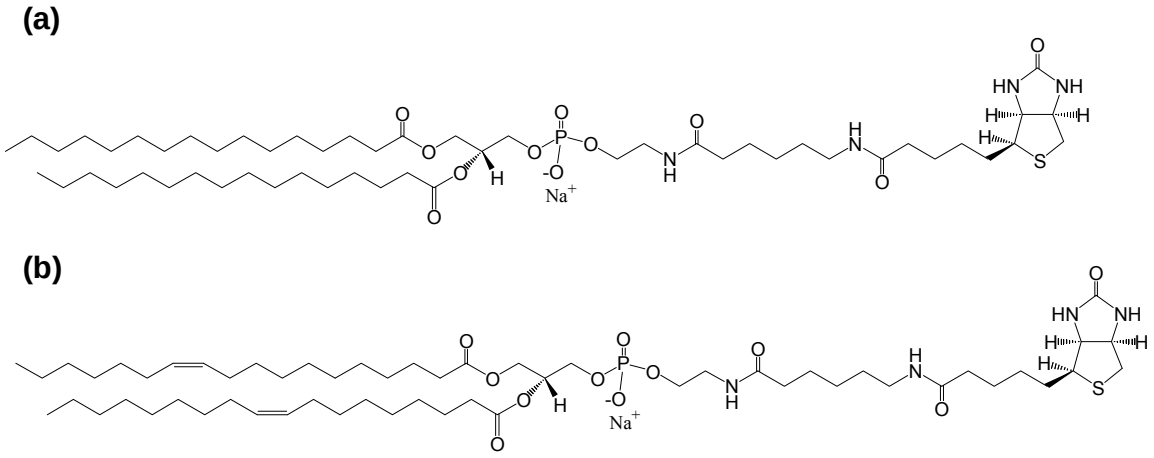

Figure 4.1. Structures: (a) biotin-DPPE and (b) biotin-DOPE.

of their lipid anchors, as shown in Figure 4.1. Biotin-DPPE has a doubly-saturated lipid anchor (DPPE) and biotin-DOPE has a doubly-unsaturated lipid anchor (DOPE). These lipids are expected to have different partitioning preferences in the presence of raft and non-raft regions in membranes as illustrated in Figure 4.2. This difference in partitioning of the two lipid anchors is then expected to affect the electro-separations. Thus, the results show that two clear bands were observed in nanorafts-containing lipid bilayers. In contrast, only one band was obtained in microrafts and no rafts-containing bilayers. Moreover, it was found that the electrophoretic mobilities (μ_i) of the two components differed in the presence of nanorafts, and the partition coefficient (K_p) of biotin-DPPE found to be about 1.6 times higher than that of biotin-DOPE. These results indicate that lipid rafts of varying size can be used to both tune and improve the resolution of the separation of membrane components using bilayer electrophoresis.

Results and discussion

Formation of supported lipid bilayers containing rafts of varying size. The representative images of supported lipid bilayers containing rafts of varying size are shown in Figure 4.3. DOPC, DPPC, and cholesterol were selected to form rafts, and all the samples were prepared with equal molar ratios of DOPC, DPPC, and cholesterol. Rafts were then formed as described in experimental section. A fluorescent probe, Texas Red DHPE was added to the ternary lipid mixtures to visualize the raft and non-raft

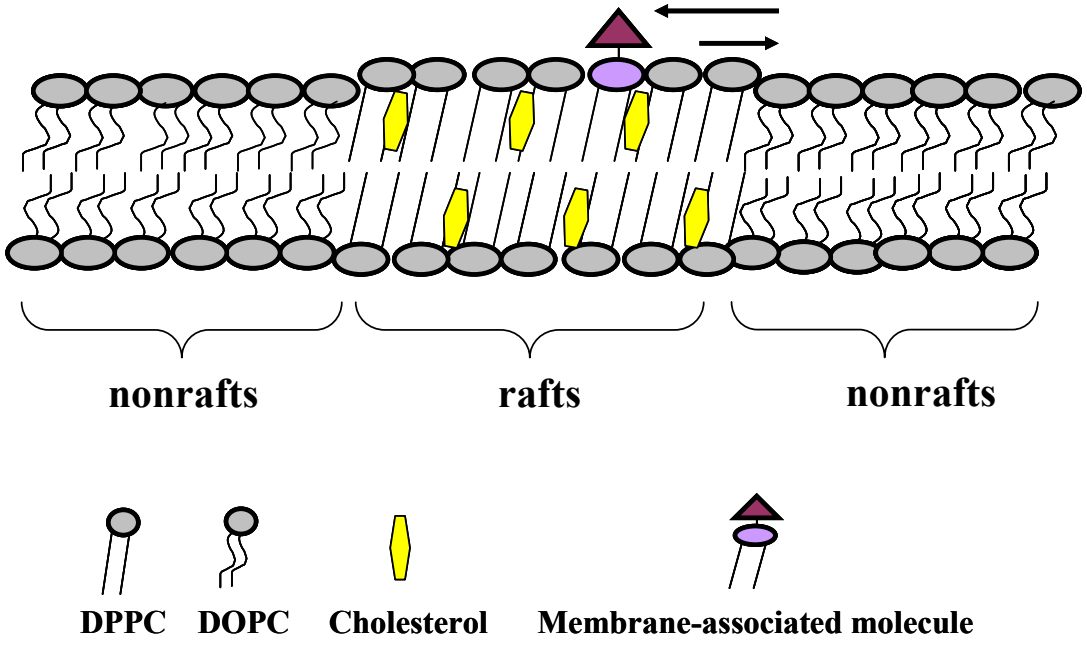

Figure 4.2. Partitioning of a membrane-anchored component between rafts and non-rafts in lipid membranes.

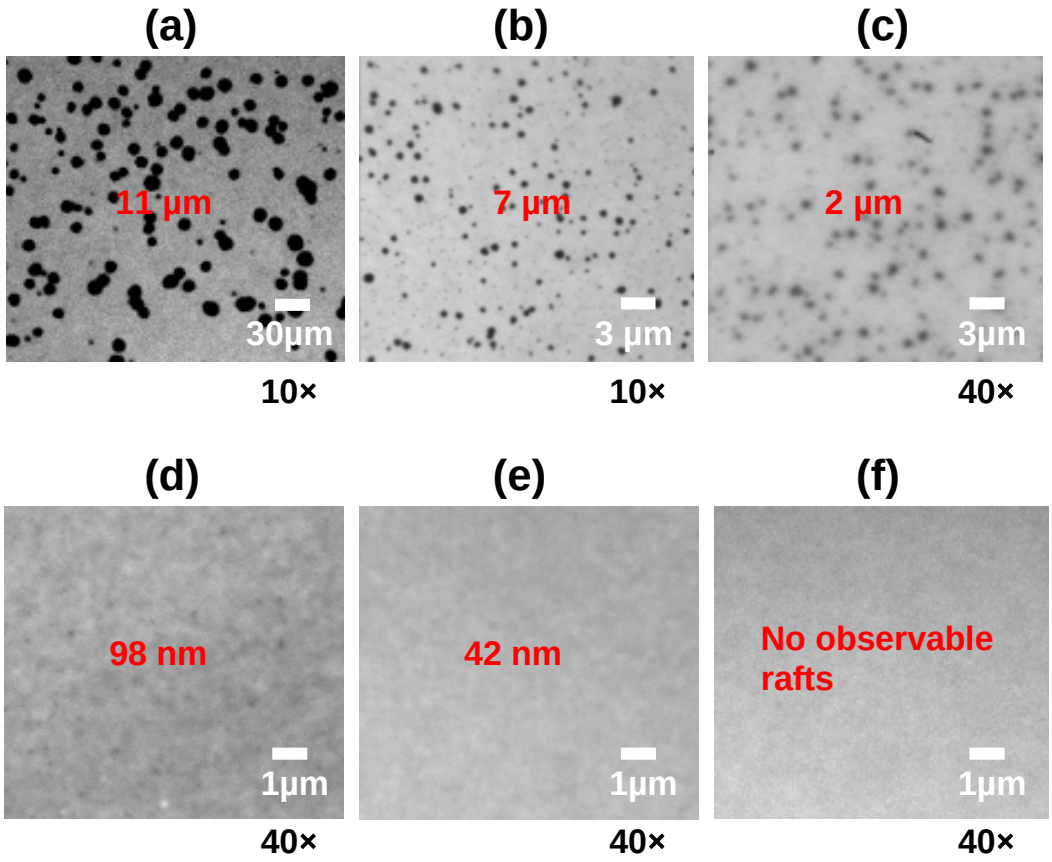

Figure 4.3. Fluorescence images of supported bilayers containing rafts with varying size. (a) Large microrafts (11 µm), (b) medium microrafts (7 µm), (c) small microrafts (2 µm), (d) nanorafts (98 nm), (e) nanorafts (42 nm), and (f) no observable lipid rafts. Rafts (dark) and non-rafts (bright) were visualized by Texas Red DHPE. The size of rafts for (d)-(f) was further characterized by AFM studies (see Figure 4). The objective used is indicated at the bottom from each micrograph.

regions in an amount of 0.03 mol %. Microraft formation involved fusing vesicles to HF-etched (5 or 10 minutes) glass substrates. It is known that the bilayers need to be heated above their phase transition temperature (T_m) to induce phase separation.[167] The ternary mixtures of equal molar ratios of DOPC/DPPC/cholesterol have T_m values around ~29 °C.[162] The supported bilayers formed on HF-etched glass were thus incubated in a hot water bath (50 °C) for 2 h and slowly cooled down to room temperature for 30 minutes. Large, circular micrometer size rafts were formed by this procedure: 11 μm with HF-etched (10 minutes) glass and 7 μm with HF-etched (5 minutes) glass, respectively (Figure 4.3a & 4.3b). The raft regions appear dark in the images due to the preferential partitioning of the Texas Red DHPE into the non-raft regions.[168] The averaged size of rafts was obtained by the estimated diameter of the dark regions in epifluorescence images at each condition. Histograms for the apparent size distribution of rafts in different experimental conditions are provided in Figure 4.5a & 4.5b. Fluorescence recovery after photobleaching (FRAP)[169] confirmed that the rafts are fluid, liquid-ordered phases. In some cases, rafts were observed to be connected, indicating that they tend to move and coalesce. This phenomenon was frequently observed in GUVs but is rare in supported bilayers.[168] It should be further noted that roughening of surfaces was not observed by HF etching, as judged by AFM measurements (see Experimental Section). When the same vesicles were fused to the piranha-etched substrate and then incubated in hot water bath for 1 h, approximately 2 μm size rafts (Figure 3c) were formed as reported by Hovis and coworkers.[151]

As pointed out in the paper, rafts were not always formed by this procedure (reproducibility: < ~ 60 %). Apparent size distribution of the rafts formed in this procedure is also provided in Figure 4.5c.

To form nanorafts, bilayers formed on baked glass substrates were incubated in hot water bath for 1 h and 25 minutes, respectively and then cooled back down to room temperature. This procedure resulted in homogeneous images down to the optical diffraction limit under what could be resolved using fluorescence microscopy with a 40× air objective (Figure 4.3d and Figure 4.3e). Therefore, in order to confirm the formation of nanorafts, AFM measurements were performed for those bilayers (see Experimental Section for detail). The results revealed that nanorafts of different size were formed depending on the heating time (Figure 4.4a & 4.4b): 98 nm-rafts were formed for 1 h heating and 42 nm-rafts for 25 minutes heating, respectively. The average size of rafts was determined from 1×1 μm^2 AFM images. Histograms for the size distribution of nanorafts are provided in Figure 4.5d & 4.5e. Interestingly, these rafts are more connected and more irregular in shape as compared to the microrafts (Figure 4.3a-c). They have ~ 0.7-1.1 nm high features which compare well with the value previously reported for supported bilayers consisting of DOPC/DPPC/cholesterol.[48] In fact, the height difference in the bilayer thicknesses of gel-phase DPPC and fluid-phase DOPC was experimentally estimated ~ 1.1-1.2 nm.[166,170] In addition, cholesterol is known to increase the length of the fluid PC molecule so that the average height difference between the rafts and surrounding non-rafts becomes slightly lower than for gel-fluid phases.[171-173]

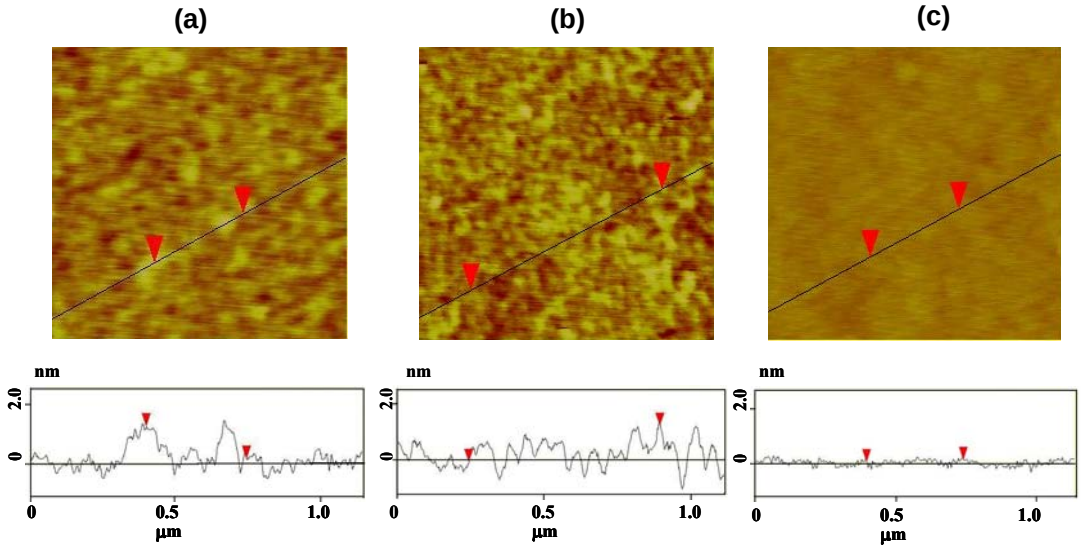

Figure 4.4. AFM images (1 µm × 1 µm) of supported lipid bilayers containing nanorafts. (a) 98 nm (1 h at 50 °C), (b) 42 nm (25 minutes at 50 °C), and (c) no observable rafts (no heat treatment).

Table 5.1. Comparison of band resolution (R_s)

Raft size	[a] S_{nr}/S_r	[b] R_s (expected)	R_s (obtained)
0 nm	0	0	0
42 nm	[c] ~ 0.8	1.5	1.5
98 nm	[c] ~ 0.6	0.7	1.0
2 μm	~ 1	0	0.6
7 μm	~ 3	0	0
11 μm	~ 5	0	0

(a) S_{nr} = surface areas of non-rafts and S_r = surface areas of rafts

(b) calculated from Purnell equation[174] as follows:

$$R_s \propto \frac{\sqrt{N}}{4}\frac{\alpha-1}{\alpha}\frac{1+k_2}{k_2}$$

where N is the average number of theoretical plates, α is the selectivity factor (K_{p1}/K_{p2}) and k_2 is the retention factor for component 2 (biotin-DOPE in this case), equal to $K_{p2}\beta$ where K_{p2} is the partition coefficient and β is the phase ratio (equal to S_{nr}/S_r in this case). We assumed that N is simply inversely proportional to the square root of particle size[175] and the value of α is independent upon the size of rafts.

(c) see the texts

This is consistent with the results that rafts formed in these experiments are liquid ordered phases and not defects or gel phases. Based on the height difference between the phases, the elevated phase is assumed to be DPPC- and cholesterol-enriched raft regions and the lower phase to be a DOPC-enriched, non-raft region.[48,176] Bilayers which were formed on baked substrates and not heated looked relatively flat and featureless (Figure 4.3e & 4.4c). Indeed, no observable rafts were found according to AFM analysis. This is consistent with previously reported ideas that the thermal history is necessary to induce phase separation in lipid bilayers.[167]

Interestingly, changes in the treatment of the solid support not only change the size of rafts, but the surface area that they cover in the bilayers. Thus, an attempt to estimate the ratio of surface areas between nonrafts and rafts in the bilayers (S_{nr}/S_r) was made. The values for microrafts could be easily estimated by assuming that all rafts are circular (dark areas in Figure 4.3a-c). The area rafts cover in nanorafts-containing bilayers is difficult to determine accurately due to the irregular shape and small size, but could be roughly estimated using a particle analysis function provided by nanoscope IIIa software (V. 5.30). These results are summarized in Table 5.1 and it is clearly shown that nanorafts form more densely than microrafts. However, it should be noted that the ratio of surface areas was not controlled in our experimental conditions.

The representative images shown in Figure 4.3 & 4.4 could be different from the matrix lipid bilayers employed in bilayer electrophoresis experiments (see below). It should be, however, noted that they are at least similar because rafts were formed from batch to batch with high reproducibility.

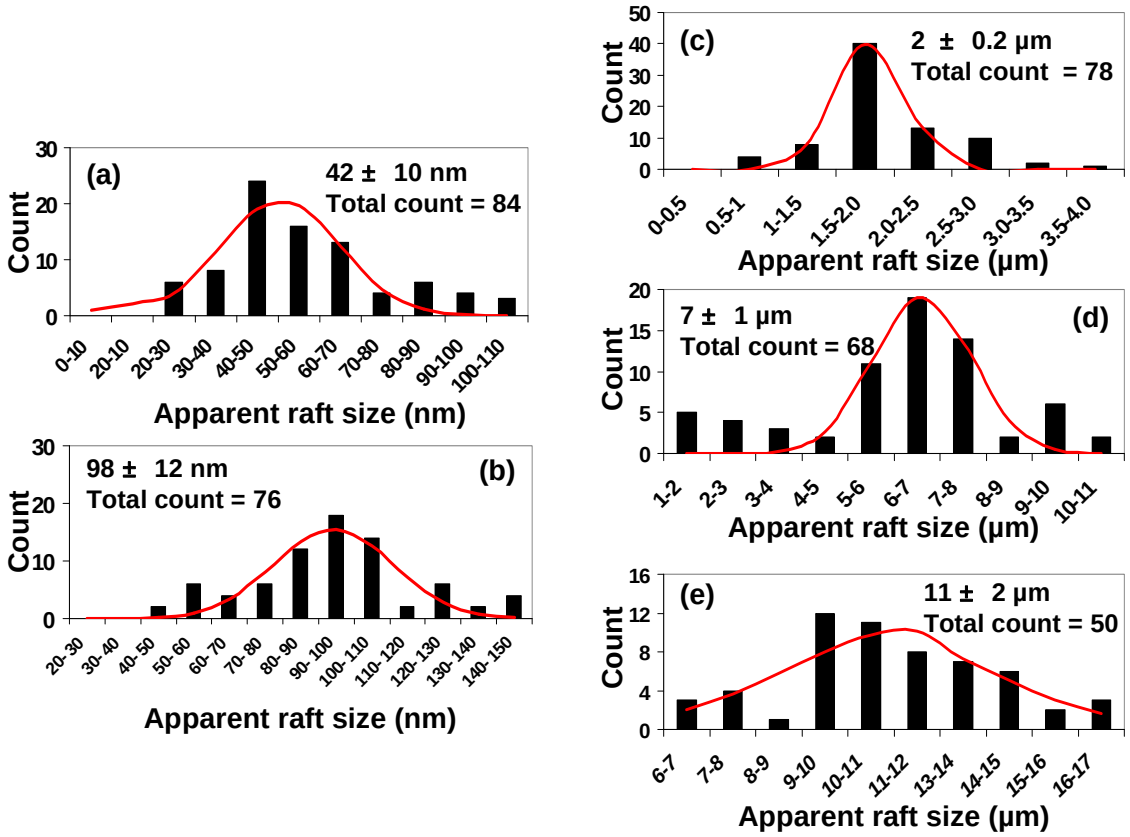

Figure 4.5. Histograms for the distribution of raft size in supported lipid bilayers. (a) nanorafts (42 nm), (b) nanorafts (98 nm), (c) small microrafts (2 µm), (d) medium microrafts (7 µm), and (e) large microrafts (11 µm). The standard deviation of the raft size was obtained by fitting to a Gaussian function. Each averaged raft size as well as standard deviation and total counts for rafts were shown in each panel.

Electrophoresis of two biotin lipids on rafts of varying size in supported lipid bilayers. The size of rafts was systematically manipulated from micrometer to nanometer as shown in Figure 4.3 and Figure 4.4. Two structurally similar membrane-anchored components, biotin-DPPE and biotin-DOPE were chosen as analytes (see Figure 4.1 for structures) to demonstrate the use of lipid rafts in electrophoresis. The experiment was performed with a 2 cm separation length controlled by a PDMS frame for 30 minutes, using a field strength of 125V/cm. The electric field lines were setup to run parallel to the bilayers and solid support and the positive and negative electrodes were located on the right and left sides of the PDMS frame, respectively. When the electric field is applied parallel to the bilayer, charged species move by either electrophoretic forces or electro-osmosis.[154] In these experiments, the phosphate group (PE) of biotin lipids ($pK_a \sim 3$)[177] is negatively charged (-1) and biotin itself is neutral. In cases where the mobile charged component is well within the electrical double layer, electro-osmosis is negligible. The Debeye screening length in our experiments is typically 1~2 nm, and the biotin molecules linked to the head group of lipids via a linker which is approximately 1.2 nm long,[178] are well within the double layer. Therefore, biotinylated lipids are expected to move by electrophoretic forces toward the positive electrode. It should be further noted that rafts which have no net charge protrude only ~ 0.7-1.1 nm above non-rafts regions in the bilayers. The electro-osmotic flow, thus, should have little effect on rafts that are present in bilayers.

After electro-separation was complete, biotinylated lipid molecules in bilayers were stained to make them visible using Alexa Fluor-594 labeled streptavidin (0.5 μM). Streptavidin is known to bind biotin molecules with a high binding affinity.[179]

The results in Figure 4.6 show that band separation depends on the size of rafts in the bilayers employed. Although the surface density of rafts was changed as well, the difference in size was more pronounced (see Table 5.1). Thus, the results will be described according to the size of rafts rather than the surface density. It was assumed that the lipid composition is independent of the size of rafts. The microrafts (7-11 μm)-containing bilayers showed substantial band broadening after 30 minutes of applied voltage. In fact, only one band was found (resolution, R_s = 0). The effect of surface roughness due to HF-etching on electrophoresis was found to be negligible. In contrast, bilayers containing 2 μm-sized rafts showed decreased band broadening and had a resolution (R_s) of 0.6. However, it should be noted that this result was reproduced poorly from batch to batch. This is probably due to the low reproducibility of raft formation as described above.

As the size of rafts decreased to the nanometer range, the separation of the two bands was significantly improved. The bands were resolved into two distinct chromatographic features with the value of R_s = 1.0 for 98 nm-sized nanorafts. The two bands were further resolved with the value of R_s = 1.5 in the bilayers containing 42 nm-sized nanorafts. Further decrease in the size of nanorafts showed no improvements in the resolution (data not shown).

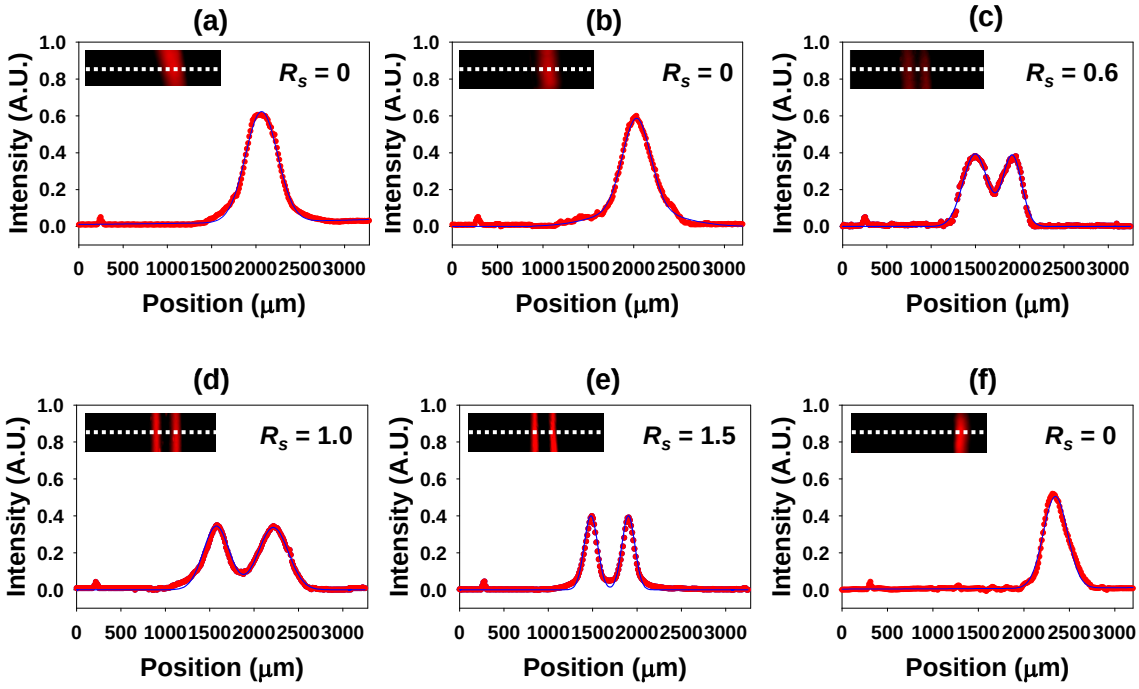

Figure 4.6. Electro-separation of biotin-DPPE and biotin-DOPE using variously-sized rafts-containing supported lipid bilayers as matrix. (a) 11 μm, (b) 7 μm, (c) 2 μm, (d) 98 nm, (e) 42 nm, and (f) no observable rafts. The fluorescence micrographs inside panels show band migration after applying 125 V/cm (DC) across the sample for 30 minutes. The small peak to the left in each image indicates the initial thin bilayer strip. The line scans (from white dotted line in fluorescence micrographs) have been corrected for vignetting and normalized to the fluorescence level of the initial peak. Each peak (red dots) from line profiles was baseline-resolved using a standard Guassian function (blue lines), resulting in band resolution (R_s) as depicted in each panel.

In order to characterize the two bands observed, biotin-DPPE and biotin-DOPE with the ratio of 1:2 (mol %) were used as analytes in the presence of 42 nm-sized nanorafts. The quantitative comparison of the area of the two analyte peaks showed that the ratio of the first and second band was approximately 1:2, indicating that the first band corresponds to biotin-DPPE and second to biotin-DOPE.

Finally, electrophoretic mobilities (μ_i) of the two biotin lipids were measured.[180] Each biotinylated lipid component (1 mol %) was exposed to lipid bilayers containing no rafts to large microrafts. Electrophoresis was performed as described in the experimental section to measure the electrophoretic mobilities. Only one band was found for all conditions as expected. The obtained values of μ_i are summarized in Table 5.2. In fact, the values of μ_i for both lipids were found to be similar either in microrafts or no raft-containing bilayers. However, the μ_i values were different in nanoraft-containing bilayers: 4.1 (± 0.5) × 10^5 $\mu m^2/(V \cdot min)$ for biotin-DOPE and 2.4 (± 0.6) × 10^5 $\mu m^2/(V \cdot min)$ for biotin-DPPE, respectively. These results suggest that the electrophoretic mobilitiy of biotin-DPPE slows down more than that of biotin-DOPE in the presence of nanorafts-containing lipid bilayers.

Partition coefficients (K_{pi}) of biotin-DPPE and biotin-DOPE. The two biotin lipids could have different partitioning preferences of their anchors into raft and non-raft regions. To investigate partitioning properties, partition coefficients (K_{pi}) for biotin-DPPE and biotin-DOPE were experimentally determined by comparing average fluorescence intensities of areas corresponding to raft and non-raft regions in the presence of two biotin lipids. It should be noted that fluorescence intensity is only

Table 5.2. Comparison of electrophoretic mobilities (μ_i)

	*Electrophoretic mobilities (μ_i, $\times 10^5$ μm^2/(V·min))	
	Biotin-DPPE	Biotin-DOPE
No rafts	- 4.4 ± 0.5	- 4.8 ± 0.5
Nanorafts (42 nm)	- 2.4 ± 0.6	- 4.1 ± 0.5
Microrafts (11 μm)	- 4.0 ± 0.6	- 4.1 ± 0.5

*Electrophoretic mobility (μ_i) was calculated with following equation:

$$\mu_i = \frac{U_i}{E}$$

where U is the migration distance per time (μm/min) and E = 125 V/cm.

dependent on the immediate environment of the probe, and insensitive to the raft size to estimate partition coefficients.[181] Thus, one partition coefficient from a certain size of rafts will represent all cases in these experiments. The resulting fluorescence micrographs and partition coefficient (K_{pi}) are shown in Figure 4.7. In this case, the raft regions appear bright. Estimates from fluorescence micrographs resulted in a partition coefficient for biotin-DPPE with the value of $K_{p1} \sim 1.6$, indicating that biotin-DPPE preferentially partitions to a detectable, albeit modest, extent into the raft regions. This is consistent with the notion that saturated fatty acyl chains partition preferentially into the less fluid membrane in the rafts.[182] In contrast, biotin-DOPE exhibits apparently no preference to partition into any regions in the bilayers, with K_{p2} value of ~ 1.0.

Not only does biotin-DPPE partition with ~ 1.6 times higher preference into raft regions than biotin-DOPE, but also biotin-DPPE molecules show slower electrophoretic mobility (μ_i) only in the matrix lipid bilayers containing nanorafts. This is consistent with previously reported observations that small obstacles are more efficient than larger obstacles at hindering diffusion.[183] In addition, nanorafts were usually formed with higher surface densities than microrafts in this study. Therefore, we suggest that the biotin-DPPE lipid molecules should encounter and interact with rafts more frequently in nanorafts-containing bilayers than biotin-DOPE. Thus, biotin-DPPE molecules will tend to remain in the nanoraft regions, and move more slowly toward the positive electrode.

Various-sized rafts are reminiscent of particles of different size in column chromatography, i.e. liquid chromatography (LC). Thus, it may be useful to relate the band resolution (R_s) obtained herein to the conventional column chromatography

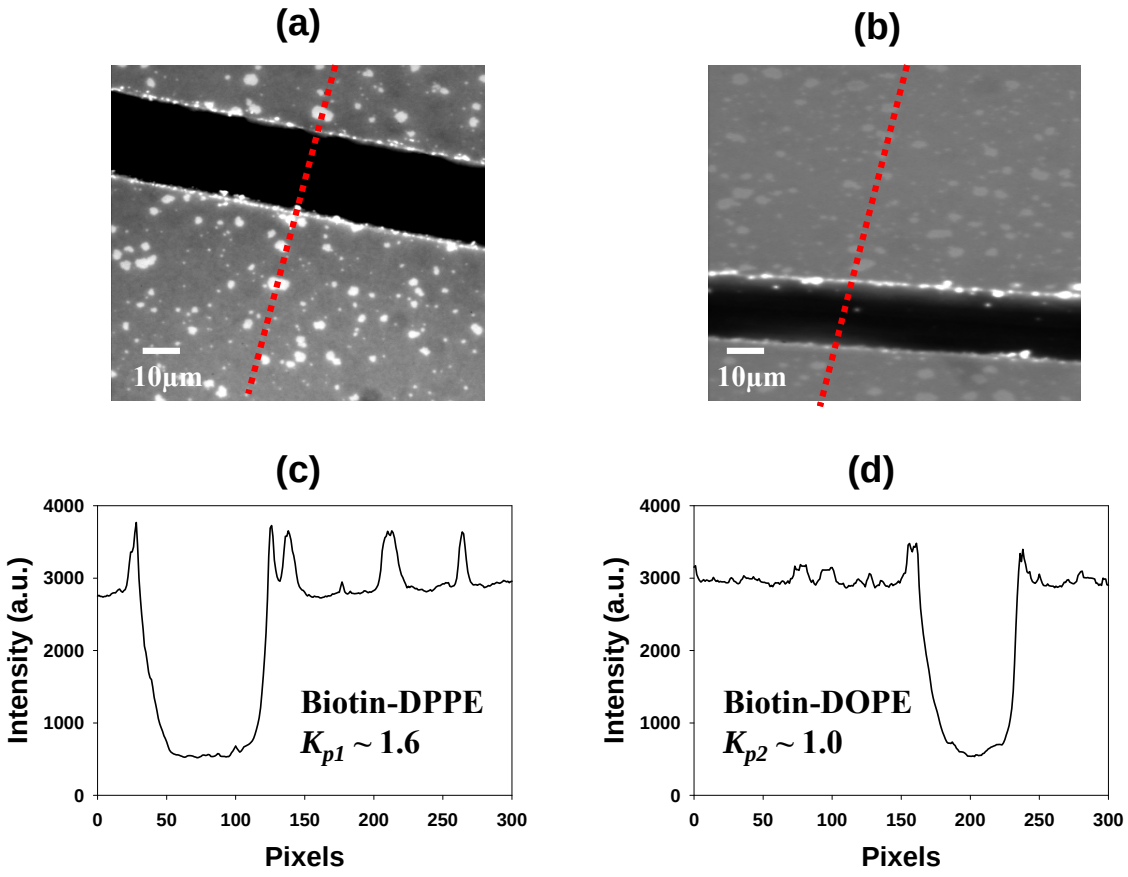

Figure 4.7. Estimation of partition coefficients (K_{pi}) for each biotin lipids between raft and non-raft regions. (a) and (b) fluorescence images for biotin-DPPE and biotin-DOPE in rafts (7 μm), respectively. 40× objective was used for images. The black lines in the images are scratches that were intentionally made with a pair of metal tweezers for the estimation of the background contribution to the measured fluorescence intensity. (c) and (d) corresponding line scans from red dotted lines in (a) and (b). K_{pi} was estimated from the background-corrected average fluorescence intensities of raft and non-raft regions in the images of the planar bilayers.

resolution equation.[174] It must be noted that this comparison is not completely accurate, as instead of a stationary phase and a mobile phase there are two phases with somewhat different mobilities. Nevertheless, the broad principles are similar enough that additional insight can be obtained. The ratio of surface areas (S_{nr}/S_r) of non-raft and raft regions in bilayers employed can be correlated to the volume ratio (V_m/V_s) of mobile and stationary phases in LC, accordingly. This simple approximation could lead us to roughly estimate resolution values, which are shown in Table 1.1. The experimentally determined values of R_s (obtained) in bilayers electrophoresis were comparable with the calculated values of R_s (expected). However, further experiments and careful analysis should be required for detailed discussion, which is beyond this paper.

Conclusion

This work reports bilayer electrophoresis using rafts of varying size as the separation media. Specifically, the electro-separation of two biotin lipid molecules with different anchors was demonstrated in the presence of variously-sized rafts on solid supported lipid bilayers. The results showed that the band resolution depends on the size of rafts in the bilayers. In particular, nanorafts-containing bilayers showed enhanced band separation with greatly reduced band widths. We suggest that the difference in partitioning of lipid anchors between raft and non-raft regions in bilayers could affect the electro-separation. Namely, lipids with doubly saturated acyl chains (biotin-DPPE) have a stronger interaction with the raft regions ($K_{p1} \sim 1.6$). In contrast, lipids with doubly unsaturated acyl chains (biotin-DOPE) have no preference for raft regions ($K_{p2} \sim 1.0$).

Indeed, biotin-DPPE lipids showed slower electrophoretic mobility than biotin-DOPE in the presence of nanorafts. These results suggest the possibility that the resolution of membrane-anchored protein separation using electrophoresis with supported bilayers can be improved by using raft-containing bilayers as demonstrated here. Finally, recent studies have proposed that the size of cell membrane rafts are likely to be less than 70 nm in diameter.[184] This corresponds with the size of rafts that allowed the two biotin molecules to be successfully separated by bilayer electrophoresis in our work. We hope our results could suggest some ideas to the current biological studies related to the rafts.

CHAPTER VI

CONCLUSION

Fluid supported lipid bilayers provide an excellent platform for studying multivalent protein-ligand interactions because the two-dimensional fluidity of the membrane allows for the lateral rearrangement of ligands to optimize binding. Our laboratory has combined supported lipid bilayer-coated microfluidic platforms with total internal reflection fluorescence microscopy (TIRFM) to obtain equilibrium dissociation constant (K_D) data for these systems. This high throughput, on-chip approach provides highly accurate thermodynamic information about multivalent binding events while requiring only very small sample volumes.

From these studies, we reported the effects of ligand presentation on the binding of aqueous proteins to solid supported lipid bilayers. Specifically, we showed that the equilibrium dissociation constant can be strongly affected by ligand lipophilicity and linker length/structure. The apparent equilibrium dissociation constants (K_D) were compared for two model systems, biotin/anti-biotin and 2,4-dinitrophenyl (DNP)/anti-DNP, in bulk solution and at model membrane surfaces. The binding constants in solution were obtained from fluorescence anisotropy measurements. The surface binding constants were determined by microfluidic techniques in conjunction with total internal reflection fluorescence microscopy. The results showed that the bulk solution equilibrium dissociation constants for anti-biotin and anti-DNP were almost identical, $K_{D(bulk)} = 1.7 \pm 0.2$ *nM* vs. 2.9 ± 0.1 *nM*. By contrast, the dissociation constant for anti-

biotin antibody was three orders of magnitude tighter than for anti-DNP at a lipid membrane interface, K_D = 3.6 ± 1.1 *nM* vs. 2.0 ± 0.2 μM. We postulate that the pronounced difference in surface binding constants for these two similar antibodies is due to differences in the ligands' relative lipophilicity. Namely, the more hydrophobic DNP molecules had a stronger interaction with the lipid bilayers, rendering them less available to incoming anti-DNP antibodies compared with the biotin/anti-biotin system. However, when membrane-bound biotin ligands were well screened by a poly (ethylene glycol) (PEG) polymer brush, the K_D value for the anti-biotin antibody could also be weakened by three orders of magnitude, 2.4 ± 1.1 μM. On the other hand, the dissociation constant for anti-DNP antibodies at a lipid interface could be significantly enhanced when DNP haptens were tethered to the end of very long hydrophilic PEG lipopolymers (K_D = 21 ± 10 *nM*) rather than presented on short lipid-conjugated tethers. These results demonstrated that ligand presentation strongly influences protein interactions with membrane-bound ligands.

Current surface binding assays routinely require fluorescently labeling the proteins of interest. However, protein labeling can interfere with detection measurements and be highly inconvenient to be employed. Herein, we described a highly sensitive technique for detecting protein-ligand binding at the liquid/solid interface. The method was based upon modulation of the interfacial pH upon protein binding. This change was detected by ortho-Texas Red DHPE, which was doped into supported phospholipid bilayers and used as a pH sensitive dye. The dye molecule fluoresces strongly at acidic pH values, but not basic ones and has an apparent pK_A of 7.8 in 1-palmitoyl-2-oleoyl-*sn*-

glycero-3-phosphocholine membranes containing 0.5 mol % biotin-cap-PE. Introducing a saturation concentration of anti-biotin antibodies to the system shifted the apparent pK_A value by 0.35 pH units. The equilibrium dissociation constant of the biotin/anti-biotin system could be determined by following the rise in fluorescence intensity at the interface as the antibody is introduced. This change was essentially linear with protein coverage under the conditions employed. Using this method, it was determined that K_D = 24 ± 5 nM for biotin/anti-biotin, which was in excellent agreement with classical measurements made by total internal reflection fluorescence microscopy involving fluorophore-conjugated antibody molecules. Moreover, the limit of detection for the label free method was ~8 pM anti-biotin in the bulk solution at the 99% confidence level. This detection limit corresponded to 380 proteins bound to the surface over a single 1.7 μm^2 sensor element area. Such results compare extremely favorably with surface plasmon resonance studies of interfacial ligand-receptor binding. In fact, the value for the detection limit is amongst the lowest known for any technique run in imaging mode. Multiple assays could be performed simultaneously by imaging a parallel array of microfluidic channels with a CCD camera.

Finally, electrophoresis using rafts-containing lipid bilayers on solid support as separation media was demonstrated. Lipid rafts of varying size were formed by a process which was controlled by varying the solid substrate (glass) treatment. Raft formation was characterized by fluorescence microscopy and atomic force microscopy (AFM). Depending on which method was employed, our results showed that the size of lipid rafts could be modulated over five orders of magnitude. Using these rafts-containing

bilayers as separation matrices, we separated two similar membrane-anchored lipid components by electrophoresis: 1,2-dipalmitoyl-*sn*-glycero-3-phosphoethanolamine-N-(cap biotinyl) (biotin-DPPE) and 1,2-dioleoyl-*sn*-glycero-3-phosphoethanolamine-N-(cap biotinyl) (biotin-DOPE). These two lipids have the same head group and same charge, but differ in the structure of their lipid anchors. It was found that the separation of the two components depended on the size of rafts in the bilayer matrix. In particular, the electrophoretic mobilities (μ_i) of the two components were found to differ in the presence of nanorafts. In addition, it is shown that the partitioning preference of biotin-DPPE into rafts was found to be about 1.6 times higher than that of biotin-DOPE. These suggest that the partitioning preference of the lipid's anchors could affect the separation during electrophoresis. These results indicate that the separation of lipid components and possibly other biological membrane components through bilayer electrophoresis can be improved through the use of lipid rafts.

REFERENCES

(1) Mammen, M.; Choi, S. K.; Whitesides, G. M. *Angew. Chem. Int. Ed.* **1998**, *37*, 2754-2794.

(2) Kiessling, L. L.; Pohl, N. L. *Chem. Biol.* **1996**, *3*, 71-77.

(3) Heldin, C. H. *Cell* **1995**, *80*, 213-223.

(4) Sabesan, S.; Duus, J. O.; Neira, S.; Domaille, P.; Kelm, S.; Paulson, J. C.; Bock, K. *J. Am. Chem. Soc.* **1992**, *114*, 8363-8375.

(5) Morgenstern, R. *Chem. Res. Toxicol.* **1998**, *11*, 703-707.

(6) Liu, X. J.; Liang, A. Y.; Shen, Z.; Liu, X.; Zhang, Y.; Dai, Z. P.; Xiong, B. H.; Lin, B. C. *Electrophoresis* **2006**, *27*, 5128-5131.

(7) Soper, S. A.; Warner, I. M.; McGown, L. B. *Anal. Chem.* **1998**, *70*, 477R-494R.

(8) Tan, P. K.; Downey, T. J.; Spitznagel, E. L.; Xu, P.; Fu, D.; Dimitrov, D. S.; Lempicki, R. A.; Raaka, B. M.; Cam, M. C. *Nucleic Acids Res.* **2003**, *31*, 5676-5684.

(9) Kim, S. R.; Abbott, N. L. *Adv. Mater.* **2001**, *13*, 1445-1449.

(10) Brake, J. M.; Daschner, M. K.; Luk, Y. Y.; Abbott, N. L. *Science* **2003**, *302*, 2094-2097.

(11) Baksh, M. M.; Jaros, M.; Groves, J. T. *Nature* **2004**, *427*, 139-141.

(12) Cui, Y.; Wei, Q. Q.; Park, H. K.; Lieber, C. M. *Science* **2001**, *293*, 1289-1292.

(13) Patolsky, F.; Zheng, G. F.; Lieber, C. M. *Anal. Chem.* **2006**, *78*, 4260-4269.

(14) Wang, W. U.; Chen, C.; Lin, K. H.; Fang, Y.; Lieber, C. M. *Proc. Natl. Acad. Sci. U. S. A.* **2005**, *102*, 3208-3212.

(15) Muratsugu, M.; Ohta, F.; Miya, Y.; Hosokawa, T.; Kurosawa, S.; Kamo, N.; Ikeda, H. *Anal. Chem.* **1993**, *65*, 2933-2937.

(16) Cooper, M. A.; Dultsev, F. N.; Minson, T.; Ostanin, V. P.; Abell, C.; Klenerman, D. *Nat. Biotechnol.* **2001**, *19*, 833-837.

(17) Yao, C. Y.; Chen, Q. H.; Chen, M.; Zhang, B.; Luo, Y.; Huang, Q.; Huang, J. F.; Fu, W. L. *J. Nanosci. Nanotechno.* **2006**, *6*, 3828-3834.

(18) Yang, C. Y.; Brooks, E.; Li, Y.; Denny, P.; Ho, C. M.; Qi, F. X.; Shi, W. Y.; Wolinsky, L.; Wu, B.; Wong, D. T. W.; Montemagno, C. D. *Lab on a Chip* **2005**, *5*, 1017-1023.

(19) Kroger, D.; Hucho, F.; Vogel, H. *Anal. Chem.* **1999**, *71*, 3157-3165.

(20) Hoffman, T. L.; Canziani, G.; Jia, L.; Rucker, J.; Doms, R. W. *Proc. Natl. Acad. Sci. U. S. A.* **2000**, *97*, 11215-11220.

(21) Song, X. D.; Swanson, B. I. *Anal. Chem.* **1999**, *71*, 2097-2107.

(22) Cremer, P. S.; Boxer, S. G. *J. Phys. Chem. B* **1999**, *103*, 2554-2559.

(23) Hlavacek, W. S.; Posner, R. G.; Perelson, A. S. *Biophys. J.* **1999**, *76*, 3031-3043.

(24) Kim, J.; Kim, G.; Cremer, P. S. *Langmuir* **2001**, *17*, 7255-7260.

(25) Yang, T.; Jung, S. Y.; Mao, H.; Cremer, P. S. *Anal. Chem.* **2001**, *73*, 165-169.

(26) Kalb, E.; Engel, J.; Tamm, L. K. *Biochemistry* **1990**, *29*, 1607-1613.

(27) Delamarche, E.; Schmid, H.; Michel, B.; Biebuyck, H. *Adv. Mater.* **1997**, *9*, 741-746.

(28) Mao, H.; Yang, T.; Cremer, P. S. *Anal. Chem.* **2002**, *74*, 379-385.

(29) Thompson, N. L.; Pearce, K. H.; Hsieh, H. V. *Eur. Biophys. J.* **1993**, *22*, 367-378.

(30) Hlady, V.; Reinecke, D. R.; Andrade, J. D. *J. Colloid Interface Sci.* **1986**, *111*, 555-569.

(31) Axelrod, D.; Burghardt, T. P.; Thompson, N. L. *Annu. Rev. Biophys. Bioeng.* **1984**, *13*, 247-268.

(32) Pisarchick, M. L.; Thompson, N. L. *Biophys. J.* **1990**, *58*, 1235-1249.

(33) Albertorio, F.; Diaz, A. J.; Yang, T.; Chapa, V. A.; Kataoka, S.; Castellana, E. T.; Cremer, P. S. *Langmuir* **2005**, *21*, 7476-7482.

(34) Shi, J.; Yang, T.; Kataoka, S.; Zhang, Y.; Diaz, A. J.; Cremer, P. S. *J. Am. Chem. Soc.* **2007**, *129*, 5954-5961.

(35) Holden, M. A.; Kumar, S.; Castellana, E. T.; Beskok, A.; Cremer, P. S. *Sensors Actuat. B* **2003**, *92*, 199-207.

(36) Jung, H. S.; Yang, T.; Lasagna, M. D.; Shi, J. J.; Reinhart, G. D.; Cremer, P. S. *Biophys. J.* **2008**, *94*, 3094-3103.

(37) Pham, A. S.; Janiak-Spens, F.; Reinhart, G. D. *Biochemistry* **2001**, *40*, 4140-4149.

(38) Pauyo, T.; Hilinski, G. J.; Chiu, P. T.; Hansen, D. E.; Choi, Y. J.; Ratner, D. I.; Shah-Mahoney, N.; Southern, C. A.; O'Hara, P. B. *Mol. Immunol.* **2006**, *43*, 812-821.

(39) Yang, T.; Baryshnikova, O. K.; Mao, H.; Holden, M. A.; Cremer, P. S. *J. Am. Chem. Soc.* **2003**, *125*, 4779-4784.

(40) Lagerholm, B. C.; Starr, T. E.; Volovyk, Z. N.; Thompson, N. L. *Biochemistry* **2000**, *39*, 2042-2051.

(41) GestyPalmer, D.; Thompson, N. L. *J. Mol. Recognit.* **1997**, *10*, 63-72.

(42) Pearce, K. H.; Hiskey, R. G.; Thompson, N. L. *Biochemistry* **1992**, *31*, 5983-5995.

(43) Thompson, N. L.; Burghardt, T. P.; Axelrod, D. *Biophys. J.* **1981**, *33*, 435-454.

(44) Daniel, S.; Diaz, A. J.; Martinez, K. M.; Bench, B. J.; Albertorio, F.; Cremer, P. S. *J. Am. Chem. Soc.* **2007**, *129*, 8072-8073.

(45) Diaz, A. J.; Albertorio, F.; Daniel, S.; Cremer, P. S. *Langmuir* **2008**, *24*, 6820-6826.

(46) Israelachivili, J. N. *Intermolecular and Surface Forces*; 2nd ed.; Academic Press: San Diego, CA, 1991.

(47) Brian, A. A.; McConnell, H. M. *Proc. Natl. Acad. Sci. U. S. A.* **1984**, *81*, 6159-6163.

(48) van Duyl, B. Y.; Ganchev, D.; Chupin, V.; de Kruijff, B.; Killian, J. A. *FEBS. Lett.* **2003**, *547*, 101-106.

(49) Evans, S. V.; MacKenzie, C. R. *J. Mol. Recognit.* **1999**, *12*, 155-168.

(50) Karlsson, K. A. *Curr. Opin. Struc. Biol.* **1995**, *5*, 622-635.

(51) Balgi, G.; Leckband, D. E.; Nitsche, J. M. *Biophys. J.* **1995**, *68*, 2251-2260.

(52) Morgenstern, R. *Chem. Res. Toxicol.* **1998**, *11*, 703-707.

(53) Liu, X.; Liang, A.; Shen, Z.; Liu, X.; Zhang, Y.; Dai, Z.; Xiong, B.; Lin, B. *Electrophoresis* **2006**, *27*, 5128-5131.

(54) Sikora, C. W.; Turner, R. J. *Biophys. J.* **2005**, *88*, 475-482.

(55) Lewinson, O.; Bibi, E. *Biochemistry* **2001**, *40*, 12612-12618.

(56) Efremov, R. G.; Chugunov, A. O.; Pyrkov, T. V.; Priestle, J. P.; Arseniev, A. S.; Jacoby, E. *Curr. Med. Chem.* **2007**, *14*, 393-415.

(57) Neves, P.; Berkane, E.; Gameiro, P.; Winterhalter, M.; de Castro, B. *Biophys. Chem.* **2005**, *113*, 123-128.

(58) Thompson, N. L.; Poglitsch, C. L.; Timbs, M. M.; Pisarchick, M. L. *Accounts. Chem. Res.* **1993**, *26*, 568-573.

(59) Pisarchick, M. L.; Thompson, N. L. *Biophys. J.* **1990**, *58*, 1235-1249.

(60) Leckband, D. E.; Kuhl, T.; Wang, H. K.; Herron, J.; Muller, W.; Ringsdorf, H. *Biochemistry* **1995**, *34*, 11467-11478.

(61) Balakrishnan, K.; Mehdi, S. Q.; McConnell, H. M. *J. Biol. Chem.* **1982**, *257*, 6434-6439.

(62) Balakrishnan, K.; Hsu, F. J.; Cooper, A. D.; McConnell, H. M. *J. Biol. Chem.* **1982**, *257*, 6427-6433.

(63) Kim, D. H.; Klibanov, A. L.; Needham, D. *Langmuir* **2000**, *16*, 2808-2817.

(64) Moore, N. W.; Kuhl, T. L. *Langmuir* **2006**, *22*, 8485-8491.

(65) Dori, Y.; Bianco-Peled, H.; Satija, S. K.; Fields, G. B.; McCarthy, J. B.; Tirrell, M. *J. Biomed. Mater. Res.* **2000**, *50*, 75-81.

(66) Klibanov, A. L.; Maruyama, K.; Torchilin, V. P.; Huang, L. *FEBS. Lett.* **1990**, *268*, 235-237.

(67) Papahadjopoulos, D.; Allen, T. M.; Gabizon, A.; Mayhew, E.; Matthay, K.; Huang, S. K.; Lee, K. D.; Woodle, M. C.; Lasic, D. D.; Redemann, C.; Martin, F. J. *Proc. Natl. Acad. Sci. U. S. A.* **1991**, *88*, 11460-11464.

(68) Lasic, D. D.; Martin, F. J.; Gabizon, A.; Huang, S. K.; Papahadjopoulos, D. *Biochim. Biophys. Acta.* **1991**, *1070*, 187-192.

(69) Torchilin, V. P.; Omelyanenko, V. G.; Papisov, M. I.; Bogdanov, A. A.; Trubetskoy, V. S.; Herron, J. N.; Gentry, C. A. *Biochim. Biophys. Acta.* **1994**, *1195*, 11-20.

(70) Bendas, G.; Krause, A.; Bakowsky, U.; Vogel, J.; Rothe, U. *Int. J. Pharm.* **1999**, *181*, 79-93.

(71) Zalipsky, S.; Puntambekar, B.; Boulikas, P.; Engbers, C. M.; Woodle, M. C. *Bioconjugate. Chem.* **1995**, *6*, 705-708.

(72) Gabizon, A.; Horowitz, A. T.; Goren, D.; Tzemach, D.; Mandelbaum-Shavit, F.; Qazen, M. M.; Zalipsky, S. *Bioconjugate. Chem.* **1999**, *10*, 289-298.

(73) Wong, J. Y.; Kuhl, T. L.; Israelachvili, J. N.; Mullah, N.; Zalipsky, S. *Science* **1997**, *275*, 820-822.

(74) Kulin, S.; Kishore, R.; Hubbard, J. B.; Helmerson, K. *Biophys. J.* **2002**, *83*, 1965-1973.

(75) Longo, G.; Szleifer, I. *Langmuir* **2005**, *21*, 11342-11351.

(76) Cooper, A. D.; Balakrishnan, K.; McConnell, H. M. *J. Biol. Chem.* **1981**, *256*, 9379-9381.

(77) Kimura, K.; Arata, Y.; Yasuda, T.; Kinosita, K.; Nakanishi, M. *Immunology* **1990**, *69*, 323-328.

(78) Ahlers, M.; Grainger, D. W.; Herron, J. N.; Lim, K.; Ringsdorf, H.; Salesse, C. *Biophys. J.* **1992**, *63*, 823-838.

(79) Jameson, D. M.; Sawyer, W. H. *Method. Enzymol.* **1995**, *246*, 283-300.

(80) Lasagna, M.; Vargas, V.; Jameson, D. M.; Brunet, J. E. *Biochemistry* **1996**, *35*, 973-979.

(81) Axelrod, D.; Burghardt, T. P.; Thompson, N. L. *Annu. Rev. Biophys. Bio.* **1984**, *13*, 247-268.

(82) Yang, T.; Baryshnikova, O. K.; Mao, H. B.; Holden, M. A.; Cremer, P. S. *J. Am. Chem. Soc.* **2003**, *125*, 4779-4784.

(83) Malencik, D. A.; Anderson, S. R. *Biochemistry* **1988**, *27*, 1941-1949.

(84) Lakowicz, J. R. *Principles of Fluorescence Spectroscopy,* Kluwer Academic / Plenum Publishers: New York, 10013, 1999.

(85) Bolger, R.; Wiese, T. E.; Ervin, K.; Nestich, S.; Checovich, W. *Environ. Heal. Pers.* **1998**, *106*, 551-557.

(86) Swillens, S. *Mol. Pharmacol.* **1995**, *47*, 1197-1203.

(87) Checovich, W. J.; Bolger, R. E.; Burke, T. *Nature* **1995**, *375*, 254-256.

(88) Mcguigan, J. E.; Eisen, H. N. *Biochemistry* **1968**, *7*, 1919-1928.

(89) Bagci, H.; Kohen, F.; Kuscuoglu, U.; Bayer, E. A.; Wilchek, M. *FEBS. Lett.* **1993**, *322*, 47-50.

(90) Tamm, L. K.; Bartoldus, I. *Biochemistry* **1988**, *27*, 7453-7458.

(91) Leckband, D. E.; Schmitt, F. J.; Israelachvili, J. N.; Knoll, W. *Biochemistry* **1994**, *33*, 4611-4624.

(92) Coreno, J.; Martinez, A.; Bolarin, A.; Sanchez, F. *J. Biomed. Mater. Res.* **2001**, *57*, 119-125.

(93) Williams, B. A.; Vigh, G. *Anal. Chem.* **1997**, *69*, 4410-4418.

(94) Kloss, A. A.; Lavrik, N.; Yeung, C.; Leckband, D. *Langmuir* **2000**, *16*, 3414-3421.

(95) Kuhl, T. L.; Majewski, J.; Wong, J. Y.; Steinberg, S.; Leckband, D. E.; Israelachvili, J. N.; Smith, G. S. *Biophys. J.* **1998**, *75*, 2352-2362.

(96) Bianco-Peled, H.; Dori, Y.; Schneider, J.; Sung, L. P.; Satija, S.; Tirrell, M. *Langmuir* **2001**, *17*, 6931-6937.

(97) Carignano, M. A.; Szleifer, I. *Macromolecules* **1995**, *28*, 3197-3204.

(98) Szleifer, I. *Biophys. J.* **1997**, *72*, 595-612.

(99) Halperin, A. *Langmuir* **1999**, *15*, 2525-2533.

(100) Kenworthy, A. K.; Hristova, K.; Needham, D.; Mcintosh, T. J. *Biophys. J.* **1995**, *68*, 1921-1936.

(101) Sheth, S. R.; Leckband, D. *Proc. Natl. Acad. Sci. U. S. A.* **1997**, *94*, 8399-8404.

(102) Kuhl, T. L.; Leckband, D. E.; Lasic, D. D.; Israelachvili, J. N. *Biophys. J.* **1994**, *66*, 1479-1488.

(103) Hanstein, W. G.; Hatefi, Y. *Proc. Natl. Acad. Sci. U. S. A.* **1974**, *71*, 288-292.

(104) 2007, http://pubchem.ncbi.nlm.nih.gov.

(105) Salerno, V. P.; Ribeiro, A. S.; Dinucci, A. N.; Mignaco, J. A.; Sorenson, M. M. *Biochem. J.* **1997**, *324*, 877-884.

(106) Livnah, O.; Bayer, E. A.; Wilchek, M.; Sussman, J. L. *Proc. Natl. Acad. Sci. U. S. A.* **1993**, *90*, 5076-5080.

(107) Clarkson, J.; Batchelder, D. N.; Smith, D. A. *Biopolymers* **2001**, *62*, 307-314.

(108) Leckband, D.; Sheth, S.; Halperin, A. *J. Biomater. Sci. Polymer. Edn.* **1999**, *10*, 1125-1147.

(109) McPherson, T.; Kidane, A.; Szleifer, I.; Park, K. *Langmuir* **1998**, *14*, 176-186.

(110) Satulovsky, J.; Carignano, M. A.; Szleifer, I. *Proc. Natl. Acad. Sci. U. S. A.* **2000**, *97*, 9037-9041.

(111) Szleifer, I. *Curr. Opin. Solid State Mater. Sci.* **1997**, *2*, 337-344.

(112) Sheth, S. R.; Leckband, D. *Proc.Natl. Acad. Sci. U. S. A.* **1997**, *94*, 8399-8404.

(113) Sheth, S. R.; Efremova, N.; Leckband, D. E. *J. Phys. Chem. B.* **2000**, *104*, 7652-7662.

(114) Cannon, B.; Weaver, N.; Pu, Q. S.; Thiagarajan, V.; Liu, S. R.; Huang, J. Y.; Vaughn, M. W.; Cheng, K. H. *Langmuir* **2005**, *21*, 9666-9674.

(115) Ebato, H.; Gentry, C. A.; Herron, J. N.; Muller, W.; Okahata, Y.; Ringsdorf, H.; Suci, P. A. *Anal. Chem.* **1994**, *66*, 1683-1689.

(116) Schneider, M. F.; Lim, K.; Fuller, G. G.; Tanaka, M. *Phys. Chem. Chem. Phys.* **2002**, *4*, 1949-1952.

(117) Porcar, I.; Codoner, A.; Gomez, C. M.; Abad, C.; Campos, A. *J. Pharm. Sci.* **2003**, *92*, 45-57.

(118) Shalmiev, G.; Ginsburg, H. *Biochem. Pharmacol.* **1993**, *46*, 365-374.

(119) Nam, J. M.; Stoeva, S. I.; Mirkin, C. A. *J. Am. Chem. Soc.* **2004**, *126*, 5932-5933.

(120) Nam, J. M.; Thaxton, C. S.; Mirkin, C. A. *Science* **2003**, *301*, 1884-1886.

(121) Stoeva, S. I.; Lee, J. S.; Smith, J. E.; Rosen, S. T.; Mirkin, C. A. *J. Am. Chem. Soc.* **2006**, *128*, 8378-8379.

(122) Brockman, J. M.; Frutos, A. G.; Corn, R. M. *J. Am. Chem. Soc.* **1999**, *121*, 8044-8051.

(123) Wegner, G. J.; Lee, H. J.; Corn, R. M. *Anal. Chem.* **2002**, *74*, 5161-5168.

(124) Lee, H. J.; Nedelkov, D.; Corn, R. M. *Anal. Chem.* **2006**, *78*, 6504-6510.

(125) Markov, D. A.; Swinney, K.; Bornhop, D. J. *J. Am. Chem. Soc.* **2004**, *126*, 16659-16664.

(126) Bornhop, D. J.; Latham, J. C.; Kussrow, A.; Markov, D. A.; Jones, R. D.; Sorensen, H. S. *Science* **2007**, *317*, 1732-1736.

(127) Song, X. D.; Nolan, J.; Swanson, B. I. *J. Am. Chem. Soc.* **1998**, *120*, 4873-4874.

(128) Song, X. D.; Nolan, J.; Swanson, B. I. *J. Am. Chem. Soc.* **1998**, *120*, 11514-11515.

(129) Yamazaki, V.; Sirenko, O.; Schafer, R. J.; Groves, J. T. *J. Am. Chem. Soc.* **2005**, *127*, 2826-2827.

(130) Zuidam, N. J.; Barenholz, Y. *Biochim. Biophys. Acta.* **1998**, *1368*, 115-128.

(131) Zuidam, N. J.; Barenholz, Y. *Biochim. Biophys. Acta.* **1997**, *1329*, 211-222.

(132) Barentholz, Y.; Hirsch-Lerner; D.; Cohen, R.; Dagan, A.; Gatt, S. U.S. Patent 7056653 B2, 2006.

(133) Corrie, J. E. T.; Davis, C. T.; Eccleston, J. F. *Bioconjugate Chem.* **2001**, *12*, 186-194.

(134) Marchesini, S.; Gatt, S.; Agmon, V.; Giudici, M. L.; Monti, E. *Biochem. Int.* **1992**, *27*, 545-550.

(135) It should be noted that the IgG molecules did not noticeably aggregate as the pH was tuned between 4 and 10.2. In fact, no changes in the activity of anti-biotin IgG were observed in the range of pH 4-10.2. This is to be expected as these proteins do not possess a single isoelectric point (pI) value as the population is polyclonal.

(136) The apparent shift of ~0.35 pH units corresponds to the relative changes in fluorescence intensity in Figure 3.3 with respect to Figure 3.5.

(137) Axelrod, D.; Burghardt, T. P.; Thompson, N. L. *Annu. Rev. Biophys. Bio.* **1984**, *13*, 247-268.

(138) Blake, R. C.; Pavlov, A. R.; Blake, D. A. *Anal. Biochem.* **1999**, *272*, 123-134.

(139) Yang, T.; Baryshnikova, O.; Mao, H.; Holden, M. A.; Cremer, P. S. *J. Am. Chem. Soc.* **2003**, *125*, 4779-4784.

(140) Christian, G. D. *Analytical Chemistry*; 6th ed.; John Wiley & Sons, Inc., New Jersey, 2004.

(141) Fromherz, P. *Method. Enzymol.* **1989**, *171*, 376-387.

(142) Fears, K. P.; Creager, S. E.; Latour, R. A. *Langmuir* **2008**, *24*, 837-843.

(143) Liang, M.; Klakamp, S. L.; Funelas, C.; Lu, H.; Lam, B.; Herl, C.; Umble, A.; Drake, A. W.; Pak, M.; Ageyeva, N.; Pasumarthi, R.; Roskos, L. K. *Assay Drug Dev. Techn.* **2007**, *5*, 655-662.

(144) White, S. H.; King, G. I. *Proc. Nat. Acad. Sci. U. S. A.* **1985**, *82*, 6532-6536.

(145) Kretschmann, E. *Z. Phys.* **1971**, *241*, 313-324.

(146) Fang, S. P.; Lee, H. J.; Wark, A. W.; Corn, R. M. *J. Am. Chem. Soc.* **2006**, *128*, 14044-14046.

(147) Goodrich, T. T.; Lee, H. J.; Corn, R. M. *J. Am. Chem. Soc.* **2004**, *126*, 4086-4087.

(148) Castellana, E. T.; Cremer, P. S. *Surf. Sci. Rep.* **2006**, *61*, 429-444.

(149) Daniel, S.; Diaz, A. J.; Martinez, K. M.; Bench, B. J.; Albertorio, F.; Cremer, P. S. *J. Am. Chem. Soc.* **2007**, *129*, 8072-8073.

(150) Suzuki, K.; Hosokawa, K.; Maeda, M. *J. Am. Chem. Soc.* **2008**, ASAP.

(151) Seu, K. J.; Pandey, A. P.; Haque, F.; Proctor, E. A.; Ribbe, A. E.; Hovis, J. S. *Biophys. J.* **2007**, *92*, 2445-2450.

(152) Groves, J. T.; Boxer, S. G. *Biophys. J.* **1995**, *69*, 1972-1975.

(153) Cremer, P. S.; Groves, J. T.; Kung, L. A.; Boxer, S. G. *Langmuir* **1999**, *15*, 3893-3896.

(154) Yoshina-Ishii, C.; Boxer, S. G. *Langmuir* **2006**, *22*, 2384-2391.

(155) Groves, J. T.; Wulfing, C.; Boxer, S. G. *Biophys. J.* **1996**, *71*, 2716-2723.

(156) Tanaka, M.; Hermann, J.; Haase, I.; Fischer, M.; Boxer, S. G. *Langmuir* **2007**, *23*, 5638-5644.

(157) Brown, D. A.; London, E. *Annu. Rev. Cell Dev. Biol.* **1998**, *14*, 111-136.

(158) Simons, K.; Ikonen, E. *Nature* **1997**, *387*, 569-572.

(159) Simons, K.; Toomre, D. *Nat. Rev. Mol. Cell Biol.* **2000**, *1*, 31-39.

(160) Sprong, H.; van der Sluijs, P.; van Meer, G. *Nat. Rev. Mol. Cell Biol.* **2001**, *2*, 504-513.

(161) Wang, T. Y.; Leventis, R.; Silvius, J. R. *Biochemistry* **2001**, *40*, 13031-13040.

(162) Veatch, S. L.; Keller, S. L. *Biophys. J.* **2003**, *85*, 3074-3083.

(163) Milhiet, P. E.; Giocondi, M. C.; Le Grimellec, C. *The Scientific World Journal* **2003**, *3*, 59-74.

(164) Ratto, T. V.; Longo, M. L. *Biophys. J.* **2002**, *83*, 3380-3392.

(165) Morandat, S.; El Kirat, K. *Langmuir* **2006**, *22*, 5786-5791.

(166) Giocondi, M. C.; Vie, V.; Lesniewska, E.; Milhiet, P. E.; Zinke-Allmang, M.; Le Grimellec, C. *Langmuir* **2001**, *17*, 1653-1659.

(167) McKiernan, A. E.; Ratto, T. V.; Longo, M. L. *Biophys. J.* **2000**, *79*, 2605-2615.

(168) Seu, K. J.; Lamberson, E. R.; Hovis, J. S. *J. Phys. Chem. B* **2007**, *111*, 6289-6292.

(169) Albertorio, F.; Chapa, V. A.; Chen, X.; Diaz, A. J.; Cremer, P. S. *J. Am. Chem. Soc.* **2007**, *129*, 10567-10574.

(170) Tristram-Nagle, S.; Petrache, H. I.; Nagle, J. F. *Biophys. J.* **1998**, *75*, 917-925.

(171) Nezil, F. A.; Bloom, M. *Biophys. J.* **1992**, *61*, 1176-1183.

(172) Saslowsky, D. E.; Lawrence, J.; Ren, X. Y.; Brown, D. A.; Henderson, R. M.; Edwardson, J. M. *J. Biol. Chem.* **2002**, *277*, 26966-26970.

(173) Rinia, H. A.; Snel, M. M. E.; van der Eerden, J. P. J. M.; de Kruijff, B. *FEBS. Lett.* **2001**, *501*, 92-96.

(174) Veatch, S. L.; Polozov, I. V.; Gawrisch, K.; Keller, S. L. *Biophys. J.* **2004**, *86*, 2910-2922.

(175) Leckband, D. E.; Schmitt, F. J.; Israelachvili, J. N.; Knoll, W. *Biochemistry* **1994**, *33*, 4611-4624.

(176) Needham, D.; Kim, D. H. *Colloids Surf. B: Biointerfaces* **2000**, *18*, 183-195.

(177) Gitlin, G.; Bayer, E. A.; Wilchek, M. *Biochem. J.* **1990**, *269*, 527-530.

(178) Zheng, S. P.; Ross, E.; Legg, M. A.; Wirth, M. J. *J. Am. Chem. Soc.* **2006**, *128*, 9016-9017.

(179) Loura, L. M. S.; Fedorov, A.; Prieto, M. *Biophys. J.* **2001**, *80*, 776-788.

(180) Milhiet, P. E.; Giocondi, M. C.; Baghdadi, O.; Ronzon, F.; Roux, B.; Le Grimellec, C. *EMBO Reports* **2002**, *3*, 485-490.

(181) Ratto, T. V.; Longo, M. L. *Biophys. J.* **2002**, *83*, 3380-3392.

(182) Said, A. S. *J. High Resolut. Chrom. Chrom. Comm.* **1979**, *10082*, 193-194.

(183) Mazzeo, J. R.; Neue, U. D.; Kele, M.; Plumb, R. S. *Anal. Chem.* **2005**, *77*, 460a-467a.

(184) Varma, R.; Mayor, S. *Nature* **1998**, *394*, 798-801.

VITA

Name:	Hyunsook Jung
Address:	Department of Chemistry, Mail Stop 3255, Texas A&M University, College Station, Texas 77843
Email Address:	hjung@mail.chem.tamu.edu
Education:	B.S., Chemistry, Hanyang University, 1996
	M.S., Chemistry, Korea Advanced Institute of Science and Technology (KAIST), 1998
	Ph.D., Chemistry, Texas A&M University, 2009